05.05.2026

River intermittency and Eocene climate change in the Castissent and Montllobat formations of the southern Pyrenean Foreland

Jonah S. McLeod[1*] (jonah.mcleod18@imperial.ac.uk)

Alexander C. Whittaker[1]

Gary J. Hampson[1]

Rebecca E. Bell[1]

Luis Valero[2]

Ziqiang Zhou[1]

[1] Department of Earth Science and Engineering, Imperial College London, SW7 2AZ, UK

[2] Departament de Dinàmica de la Terra i de Oceà, Faculty of Earth Science, University of Barcelona, Martí i Franqués, s/n, 08028 Barcelona

Funding Statement: This work was supported by the Natural Environment Research Council (Grant NE/S007415/1) and Terrabotics (London).

Conflict of Interest Statement. The authors declare no conflict of interest.

Data Availability Statement: The data that supports the findings of this study are available in the supplementary material of this article, which is available upon request.

ABSTRACT

Patterns of river water and sediment transport through time, or river intermittency factors, are generally considered to be highly sensitive to climate and tectonics. Determining the intermittency of rivers in ancient hothouse climates could provide a unique lens through which to investigate Earth's response to climate change. However, this requires strong constraints

on both mean and bankfull sediment and water discharges through time, which are rare in the stratigraphic archive due to the challenges of estimating material flux rates from source to sink. To address these challenges, we calculate basin-scale sediment volumetrics and palaeohydraulics to reconstruct water and sediment transport patterns in strata deposited under an ancient extreme climate punctuated by hyperthermal warming events: the Montllobat (52.0 – 50.5 Ma) and Castissent (50.5 – 49.7 Ma) formations of the Southern Pyrenees, during the Eocene hothouse. We reconstruct water intermittency factors (I_w) in these ancient river systems averaging 0.15-0.25, whereas sediment intermittency factors (I_s) of $3x10^{-3}$ – $7x10^{-3}$ in the Montllobat Formation increased up to 3-fold in the overlying Castissent Formation. This implies that whilst rivers were likely perennial, sand-grade sediment was transported significantly more often in the Castissent rivers ($p<10^{-3}$). A comparison with a global database of modern rivers also demonstrates that rivers during the Early Eocene Climatic Optimum were able to transport sediment more efficiently than most modern rivers of similar types and climate zones today. We hypothesise that a short-lived global warming event at c. 50.5 Ma enhanced monsoon seasonality in the Pyrenean foreland, causing heightened sediment transport efficiency which lasted up to 1 million years. This ancient example shows the long-lasting, basin-wide geomorphic consequences of short-term climatic change, resolved from river transport patterns in alluvial stratigraphy.

1 INTRODUCTION

Across the planet and throughout time, landscapes and sedimentary basins respond to climate and tectonic forcings (Knox, 1984; Bull, 1991; Tucker & Slingerland, 1997; Westra *et al.*, 2014; Yin *et al.*, 2023). Rivers, the most significant conduits of water, sediment and nutrients across Earth's continents, are particularly sensitive to climate change (Knox, 1993; Whittaker, 2012), and they provide a lens through which to investigate surface processes during extreme climate episodes of Earth's past. Present-day climate change threatens significant geomorphic ramifications (e.g., Alfieri *et al.*, 2017; Best, 2019), and decoding how Earth's surface has

53 responded to climates of the past provides one way to constrain the future impacts of global
54 warming.

55 It is widely recognised that runoff regimes, discharge variability and river hydrographs are
56 strongly determined by weather patterns driven by climate, and are vital to understanding river
57 and landscape response to allogenic drivers from millennial to sub-daily timescales (Haines
58 *et al.*, 1988; Nicholas *et al.*, 2016; Hansford *et al.*, 2020). Signals of climate-driven hydrological
59 change can be preserved in alluvial stratigraphy (Allen, 2008), and deciphering the patterns
60 of past river transport and discharge variability in the rock record is a critical way to reconstruct
61 the impact of past climate change on the Earth's surface. Alluvial stratigraphy contains
62 geological observables that can be used to reconstruct both formative depositional conditions,
63 and mean transport rates in ancient rivers. Employing empirically- and theoretically-derived
64 numerical models and relations (e.g., Leclair & Bridge, 2001; Bradley & Venditti, 2017; Lyster
65 *et al.*, 2020, 2021; Long, 2021), the architecture, bedforms and grain-sizes associated with
66 channel-fill and in-channel bar deposits can be employed to estimate key river characteristics
67 and behaviour such as flow depth, channel gradient, river planform, and water and sediment
68 discharge. Further, a range of downstream- and upstream-focused approaches are available
69 to reconstruct long-term average water and sediment fluxes (e.g., Lyster *et al.*, 2020; Watkins
70 *et al.*, 2020; Yan *et al.*, 2025). To constrain the temporal patterns of river activity in response
71 to allogenic perturbations, we can extend previous approaches based on facies and
72 stratigraphic analyses (e.g., Flood & Hampson, 2014; Fielding *et al.*, 2018; Lyster *et al.*, 2020;
73 Wood *et al.*, 2022) by directly comparing two key parameters that can be reconstructed from
74 independent geological observations: the maximum channel-forming transport flux and the
75 long-term average conditions.

76 River intermittency factors (I), introduced by Paola *et al.* (1992), describe the temporal
77 distribution of water or sediment transport through rivers which can be presented as a simple
78 ratio between the total flux over a set time scale and the potential bankfull flux if it were

sustained over the same period—in other words, how much water or sediment a river is moving versus what it could be moving (Fig. 1A):

$$I = \frac{\sum Q_{s,w}(t)}{Q_{s,w(bf)} \sum t} , \quad (1)$$

where $\sum Q_{s,w}$ is the sum of the sediment or water discharge over time period t, and $Q_{s,w(bf)} \sum t$ is the potential bankfull sediment or water discharge multiplied by the sum of the time period. This can be reformulated as:

$$I = \frac{Q_{s,w(avg)}}{Q_{s,w(bf)}} , \quad (2)$$

where $Q_{s,w(avg)}$ is the average sediment or water discharge over an arbitrary long timescale and $Q_{s,w(bf)}$ is the bankfull transport capacity of water or sediment if applied for the identical timescale.

Intermittency factors are strongly indicative of river processes and climate (McLeod *et al.*, 2026), and reconcile the critical gap in timescales between reconstructions of instantaneous channel-forming and mean flow conditions (Lyster *et al.*, 2023). Intermittency factors do not rely on assumptions of hydrograph shape, because for a given intermittency factor the integral of the hydrograph could be distributed across an infinite number of shapes and could be applied on any timescale (Fig. 1B, C). In general, however, with decreasing intermittency factor (approaching zero), rivers are expected to concentrate activity in shorter, isolated periods of discharge, separated by longer periods of low or no discharge—this would be considered an ephemeral or intermittent river. Intermittent rivers (generally considered to have measurable water discharge <10% of the time; Hedman & Osterkamp, 1982) corresponding to water intermittency (I_w) < 0.1, are associated with particular climate characteristics (Hansford *et al.*, 2020). A high intermittency factor approaching 1, on the other hand, means water discharge is perennial. Sediment hydrographs can be characterised by intermittency factors in the same

way: where sediment discharge is concentrated into infrequent, extreme events in which transport thresholds are surpassed, the ratio between $Q_{s(avg)}$ and $Q_{s(bf)}$, I_s, is likely to be close to zero (e.g., Fig. 1B, D, E). A river transporting sediment year-round will have a high I_s value approaching unity (e.g., Fig. 1C).

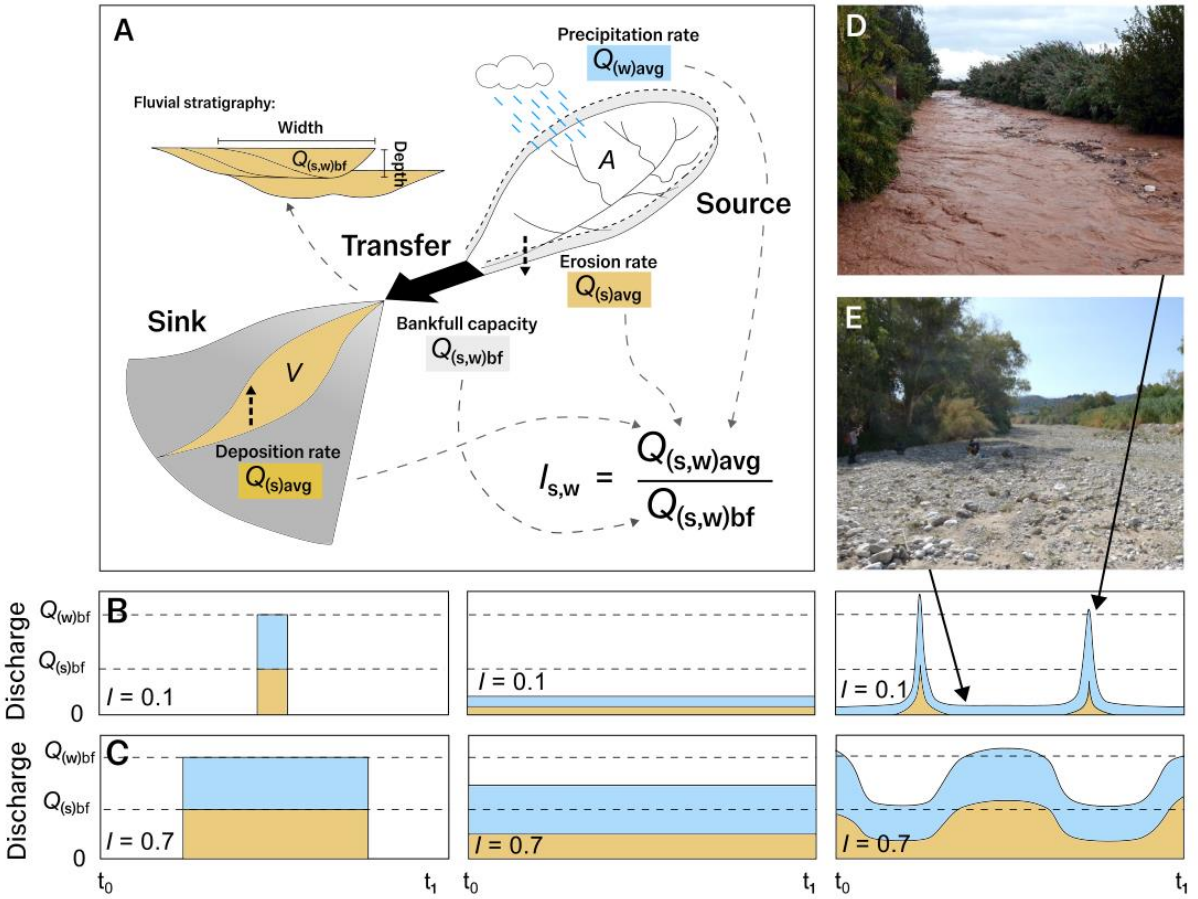

Figure 1. Diagrams outlining intermittency factors. A) Conceptual illustration highlighting the intermittency factor formula and its inputs where source — or upstream — approaches are used to estimate precipitation and erosion rates, sink — or downstream — approaches are used to estimate deposition rate, and palaeohydrology of alluvial deposits are used to estimate bankfull water and sediment transport capacity. B) Schematic hydrograph illustrating the potential hydrograph shapes for a low intermittency factor of I=0.1, where t_1-t_0 is an arbitrary time-step containing variability, for example 1 year; the blue area represents the water hydrograph and the beige area represents the sediment hydrograph. As long as the integrated area of the hydrograph is maintained, a given intermittency factor could indicate an infinite number of hydrograph shapes. C) Schematic hydrograph illustrating the potential hydrograph shapes for a high intermittency factor of I=0.7. (D-E) Photographs of ephemeral rivers in Greece at bankfull discharge (D) and during low or no flow stages (E) (McLeod *et al.*, 2024).

Recent investigations of modern rivers demonstrate water intermittency factors are globally linked to climate (McLeod *et al.*, 2026), and that sediment fluxes in arid regions are tied to individual rare storms, suggesting that sediment budgets in Mediterranean catchments could

double by 2100 CE as a consequence of global warming (McLeod *et al.*, 2024). If river intermittency responds to allogenic forcing, then it should also be possible to resolve ancient landscape-scale climate and tectonic change from the alluvial archive, and contextualise future changes to river transport patterns due to global warming, which could dramatically alter the carbon and nutrient cycle (Dunne *et al.*, 2007; Goñi *et al.*, 2013). New data describing water and sediment intermittency in modern systems worldwide (Hayden *et al.*, 2021; McLeod *et al.*, 2026) in theory enable calibration of interpretations of ancient tectonic and climatic conditions from fluvial intermittency. However, constraints on the intermittency of both river water and sediment transport are rare in the geological record, because they require estimated bankfull material fluxes to be tied directly with corresponding mean fluxes in space and time (Lyster *et al.*, 2023). In practice, this means robust, high-resolution stratigraphic correlations are required between alluvial strata and strata located downsystem in the corresponding depositional sink (Watkins *et al.*, 2019; McLeod *et al.*, 2024), and/or or well-constrained reconstructions are required for palaeo-catchment areas and climates (Lyster *et al.*, 2023). It also remains untested whether water or sediment transport patterns in ancient rivers exposed to external perturbations were affected to a degree that has stratigraphic preservation potential.

In order to address these research gaps, this paper aims to: (1) develop a framework to estimate basin-scale depositional volumes and long-term water and sediment fluxes through time in an Eocene source-to-sink system during an extreme hothouse period; (2) calculate evolving water and sediment intermittency factors in this stratigraphic setting; and (3) leverage reconstructed intermittency factors and palaeohydrological observations to determine landscape response to an Eocene global warming event. Using palaeohydrological techniques in parallel with geological and modelling approaches, we show that it is possible to reconstruct the evolving patterns of river activity in response to changes in climatic boundary conditions from the alluvial sedimentary record, using the stratigraphy of the Spanish Pyrenees as a natural laboratory.

2 GEOLOGICAL BACKGROUND

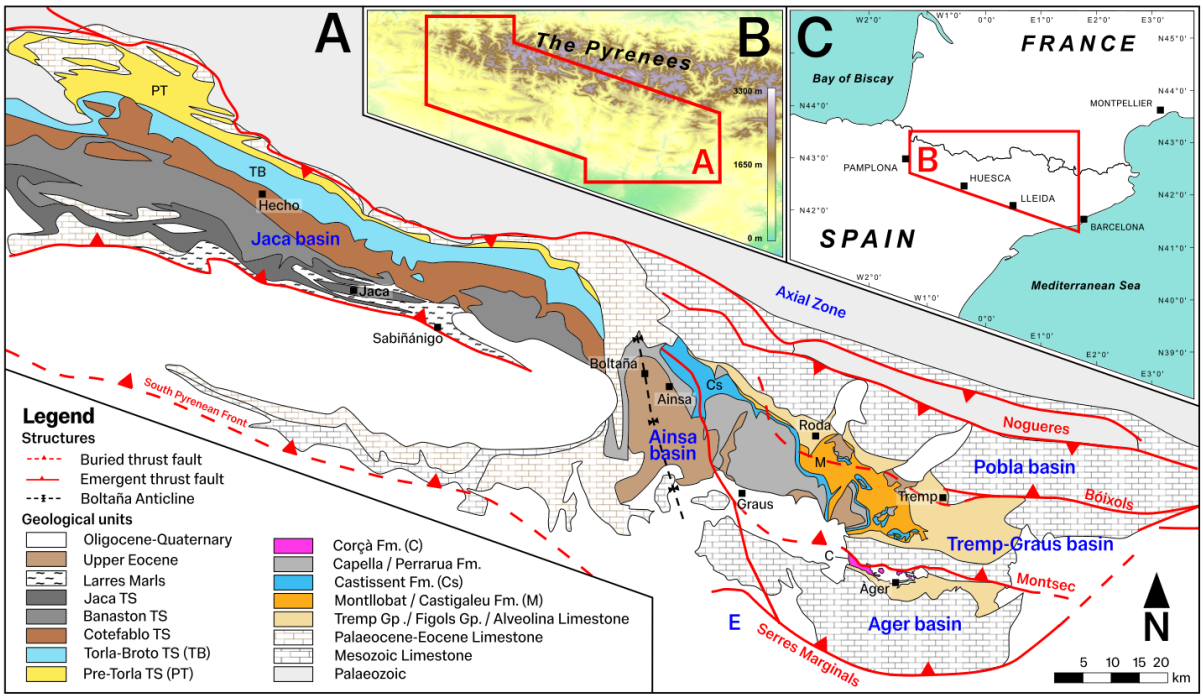

Figure 2. Study area geological and location maps in the southern Pyrenees. A) Geological sketch map highlighting the key sedimentary units of the Ypresian. B) Digital elevation model of the present-day Pyrenees. C) Geographical location map.

The Pyrenees are a NW-SE-oriented compressional mountain belt on the boundary between the Iberian and European plates (Fig. 2). The Alpine orogenic history of the Pyrenees was initiated in the late Cretaceous, when seafloor spreading in the southern Atlantic and Indian oceans drove northwards motion of the Iberian plate, resulting in the onset of convergence between the Iberian and European plates (Capote *et al.*, 2002; Martín-Chivelet *et al.*, 2002). Owing to prior Mesozoic crustal extension and attenuation, crustal loading and flexural subsidence formed deep, narrow foreland basins on both the Iberian and European sides of the mountain belt (Clark *et al.*, 2017). Exhumation of the Axial Zone of the Pyrenees continued through the late Cretaceous, and the southward propagation of a foreland fold-and-thrust belt caused the redistribution of sediment through a series of piggy-back basins Compression continued into the Palaeocene, Eocene,Oligocene and upper Miocene, until regional convergence shifted to the southern margin of the Iberian plate by the Neogene (Clark *et al.*, 2017).

The South-Central part of the Pyrenean foreland is characterized by thin-skinned thrusting on Triassic and Paleogene evaporite decollements or basement-involved thrusting, in those sectors where salt levels are lacking, both often connected laterally by oblique fault zones (Muñoz et al., 2025). Three major thrust sheets can be recognized, which by order of emplacement, are: the Cotiella-Bòixols thrust sheet, starting its emplacement by late Cretaceous; the Peña Montañesa-Montsec sheet, starting in the Paleocene up to the Late Ypresian; and the Sierras Exteriores–Serres Marginals sheet, emplaced from the Lutetian to the Lower Miocene (Simó et al., 1985; Simó, 1986; Oliva-Urcia et al., 2019). The Eocene foreland basin can be divided into four sub-basins, governed by the evolving thrust sheets and their transfer zones: the Tremp-Graus, Àger, Ainsa, and Jaca basins (Garcés et al., 2020). These four zones contained the major sediment routing systems of the South-Central Pyrenees Foreland Basin in the lower Eocene.

The Ypresian Montanyana Group (Nijman & Nio, 1975; also “Montañana Group”), represents the first major phase of clastic sedimentation and alluvial progradation driven by Pyrenean orogenesis. The first two megasequences of the Montanyana Group correspond to the fluvial Montllobat and Castissent formations (Nijman & Nio, 1975; Nijman & Puigdefàbregas, 1977; Nijman, 1998), which are the focus of this study. The Montanyana rivers of the Tremp-Graus basin transported sediment downsystem (northwest) into a shallow-marine setting dominated by deltaic mouth bars (Marzo *et al.*, 1988). In the Ainsa Basin, marine siliciclastic and carbonate slope facies are incised by deep, composite submarine canyon fills (Marzo *et al.*, 1988; Nijman, 1990; Ayckbourne *et al.*, 2024). Siliciclastic submarine channel sediments were routed into the marine Hecho Group of the Jaca basin (Mutti, 1985a), which contains coarse turbiditic lobes, distal turbidite deposits and Mega Turbidite (MT) beds (Labaume *et al.*, 1987; Labaume *et al*., 2016) on which various correlative schemes for the Jaca Basin are based. We discuss this fluvial-to-submarine-fan correlation framework, variations upon it, and their potential implications in detail in Section 3.1, and provide alternative stratigraphic correlation schemes in the Supplementary Material (Fig. S2).

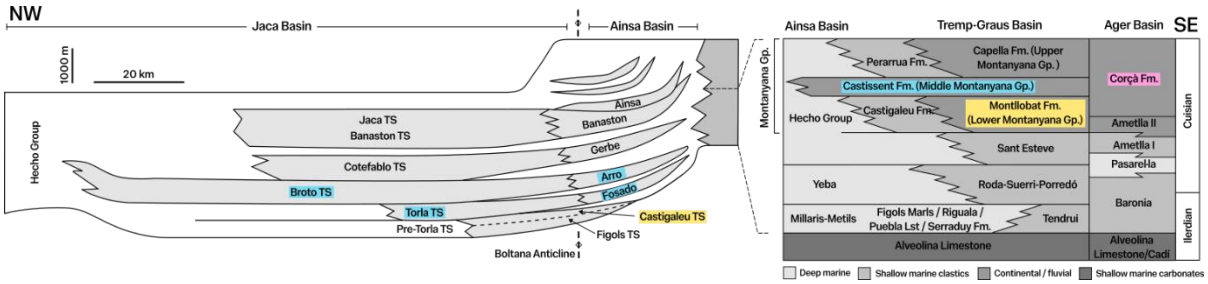

Figure 3. Stratigraphic framework for the lower Eocene units of the southern Pyrenean foreland in the Jaca, Ainsa, Tremp-Graus and Àger basins (modified after Mutti, 1985a; Labaume *et al.*, 1987; Gupta & Pickering, 2008; Caja *et al.*, 2010; Scotchman *et al.*, 2015; Garcés *et al.*, 2020). Variations on this framework could arise from different age-date interpretations and unit correlations. An alternative correlative scheme is provided in the Supplementary Material and discussed in Section 5.2.

Deposition of the Ypresian Montllobat and Castissent formations of the Lower and Middle Montanyana Group coincided with the later part of the Early Eocene Climatic Optimum (EECO) (Westerhold & Röhl, 2009; Hyland & Sheldon, 2013), with global temperatures gradually decreasing from a hothouse state that persisted through the start of the Ypresian. Global mean annual temperatures (MAT) in the EECO were approximately 23-29°C (Westerhold & Röhl, 2009; Honegger *et al.*, 2020), compared to 14-15°C in the present-day. Humidity reconstructions from CaO/Al_2O_3 ratios in Castissent Formation palaeosols indicate the climate of the southern Pyrenean foreland during the Ypresian was semi-arid (Honegger *et al.*, 2020). The lower Eocene climate was also characterised by hyperthermal events, short-duration (40-200 kyr) periods of global warming which punctuated the overall, long-term cooling trend of the late EECO (Lourens *et al.*, 2005; Kirtland Turner *et al.*, 2014; Westerhold *et al.*, 2017; Turner, 2018; Honegger *et al.*, 2020). These hyperthermal events are hypothesized to have affected continental sedimentation and fluvial dynamics in the Eocene Pyrenean foreland (Honegger *et al.*, 2020; Boyrie *et al.*, 2025; McLeod *et al.*, 2025).

The Montllobat Formation comprises the Ypresian fluvial deposits of the Lower Montanyana (LM) Group in the Tremp-Graus basin. Approximately 150-250 m thick, it is composed of overbank mudstones interbedded with channelised sandstone and conglomeratic bodies (Nijman & Nio, 1975). The fluvial channel-fill deposits include structureless kilometre-wide sheetflood deposits (Van der Meulen, 1989), multi-lateral and multi-storey sandstone bodies with well-developed lateral (point-bar) accretion (Nijman & Nio, 1975; Cabello *et al.*, 2018),

and both simple and multi-storey ribbon channel bodies (Nijman & Nio, 1975). The petrographic composition of the Montllobat Fm. is characterised by alluvial fan supply from the northern margin of the basin (Nijman, 1998). New palaeohydrological reconstructions (McLeod *et al.*, 2025) show palaeo-river flow depths averaged 1.40 m across the Tremp-Graus Basin, and field-based reconstructions indicate the median channel gradient was ca. $8.0x10^{-4}$ (m/m), with a median bedload grain-size of medium sand (0.38 mm). The Montllobat Formation has been interpreted to represent a mostly wandering or anastomosing multi-threaded river system (Van der Meulen, 1989; McLeod *et al.*, 2025) with distinct meandering reaches (Van Eden, 1970; Nijman & Nio, 1975; Puigdefabregas & Vliet, 1977; Cabello *et al.*, 2018). The Montllobat Formation is subdivided by the Mid-Lower Montanyana (MLM) unconformity, which marks a sequence boundary (Nijman, 1998), and the two subdivisions are referred to herein as Montllobat members A and B (McLeod *et al.*, 2025). With dominantly north-west-directed palaeocurrents, the Montllobat rivers pass downsystem into the shallow-marine clastic deposits of the Castigaleu Formation (Van Der Meulen, 1986).

The Montllobat Formation is overlain by the Castissent Formation, a widespread, comparatively thin (50-150 m) fluvial unit comprising the alluvial deposits of the Middle Montanyana (MM) Group. The Castissent Formation represents pronounced progradation of the Montanyana clastic wedge (Nijman & Puigdefàbregas, 1977; Marzo *et al.*, 1988; Nijman, 1998), which has been attributed to an increase in hinterland tectonic uplift rates (Whitchurch *et al.*, 2011; Curry *et al.*, 2021) and/or a climatic change (Honegger *et al.*, 2020; McLeod *et al.*, 2025). The Castissent Formation, like the underlying Montllobat Formation, comprises mottled overbank mudstone deposits and channelised fluvial sandstones (Marzo *et al.*, 1988). Its petrographic composition is carbonate-poor in comparison to the Montllobat Formation (Nijman, 1998), with a white-weathering appearance and rounded exposure style that distinguishes it from the other units of the Montanyana Group in the Tremp-Graus basin. The fluvial deposits of the Castissent Formation are dominantly multilateral and multi-story sheet sandstones, with some coarser conglomeratic channel fills. The fluvial deposits include

lenticular-bedded sheet sandstone bodies, tabular bodies containing lateral-accretion and ribbon-like channel fills (Marzo *et al.*, 1988). The Castissent Formation is composed of three main coarse-grained channel complexes (members A, B and C) separated by marine incursions (Marzo *et al.*, 1988; Honegger *et al.*, 2020), and these represent successive alluvial depositional phases (Martinius, 2012). The Castissent rivers were 1.40 m deep on average, but in contrast to the Montllobat Formation, they were developed on a steeper gradient ($1.2x10^{-3}$) and they transported a coarser bedload of coarse sand averaging 0.94 mm (McLeod *et al.*, 2025). The Castissent rivers have been interpreted as braided (Nijman & Puigdefàbregas, 1977; Marzo *et al.*, 1988; McLeod *et al.*, 2025), and McLeod *et al.* (2025) reconstructed an increase in water and sediment discharge in comparison to the underlying Montllobat Formation, reaching maximum transport capacity in Castissent member B.

Fluvial sedimentation also occurred south of the Montsec Thrust in the Àger Basin, coeval to the Montllobat and Castissent rivers (Nijman, 1998). Cropping out in the Serres Marginals thrust sheet (Fig. 2), the depositional duration of the Corçà Formation was equivalent to, or strongly overlapping with, that of the Montllobat and Castissent formations (Nijman, 1998; Juvany *et al.*, 2024) (Fig. 3). The Corçà Formation is comprised of stacked sheet sandstone complexes with north- to north-west-directed palaeocurrents, and a distinctly white-weathering exposure style, bearing notable similarities at outcrop to the Castissent Formation. The petrographic composition of the Corçà Formation suggests significant mixing with the Castissent Formation, supported by detrital zircon geochronology (Clark *et al.*, 2017; Thomson *et al.*, 2017). This mixing implies the two river systems had a similar source terrane, and they have been interpreted to effectively represent components of the same axial sediment routing system (Nijman, 1998; Martinius, 2012). The precise sediment routing palaeogeography, however, may be more nuanced. The routing system was split around the emergent Montsec Thrust (Martinius, 2012; Garcés *et al.*, 2020; Juvany *et al.*, 2024), but since transitional-to-shallow-marine Corçà deposits do not outcrop in the Àger Basin, the down-system continuation of the Corçà river's course is unclear. The compositional differences between the

Corçà and Montllobat formations (Nijman, 1998) suggest lower degrees of mixing earlier in the Ypresian. Uncertainties in the source regions of the Castissent and Montllobat formations, their catchment areas in relation to those of the Corçà Formation, and the size of their depositional sinks have the potential to affect interpretations of foreland-scale sedimentary dynamics, including our intermittency analyses. We outline our approach to addressing this uncertainty in the Methods section, below.

3 METHODS

In Section 3.1 we outline our methodology for reconstructing the depositional volumes of the early Eocene sediment routing systems, first detailing our stratigraphic correlations and subsequently describing our approaches to estimating sandstone thicknesses and calculating sediment volumetrics. In Section 3.2 we provide our methods for estimating both bankfull and mean water and sediment fluxes. These methods include utilising basin volumetrics to estimate mean sediment flux and calculations of mean water flux, followed by a description of our field-based workflow for palaeohydrological reconstruction of bankfull water and sediment discharge. We also outline our approach to addressing uncertainties, including those arising from multiple potential scenarios for specific sediment routing palaeogeographies in the Tremp-Graus and Àger basins. These methods permit the quantification of foreland-scale transport dynamics of river water and sediment during the Eocene hothouse, providing the first insights to date into river transport patterns in the southern Pyrenean foreland.

3.1 Sediment volumes

Stratigraphic correlation

Understanding transport patterns using intermittency factors — a ratio between bankfull or maximum rates and average conditions — requires the calculation of long-term water and sediment discharge rates and instantaneous (bankfull) transport capacities. In order to estimate basin sediment volumes and therefore long-term averaged sediment fluxes in the Eocene Pyrenees, we first isolated the target stratigraphic intervals. As outlined above, the

stratigraphic frameworks of the Tremp-Graus, Ainsa, and Jaca basins are extremely well-developed individually. However, the Boltaña Anticline, situated west (down-system) of the Ainsa Basin (Fig. 2), has removed most sediment of Montanyana age from this region due to post-depositional erosion. As a consequence, stratigraphic correlation across the Boltaña Anticline, between the Ainsa and Jaca basins, is challenging and associated uncertainties have resulted in differing published interpretations. We conducted a survey of existing stratigraphic correlations based on measured sedimentary logs and outcrop sections. Below, we outline the stratigraphic correlations used to estimate depositional volumes for our intermittency analysis, and we provide an alternative correlation framework in the Supplementary Materials (Fig. S2).

The last shallow-marine carbonate deposition in the Tremp-Graus and Àger basins before the onset of major stable siliciclastic input was the Ilerdian Alveolina Limestone Formation, directly overlain by the Fígols Formation and related strata that record alluvial fan and delta progradation (Fig. 3). The rivers of the Montanyana Group in the Tremp-Graus Basin transported sediment downsystem (northwest) into a shallow-marine setting dominated by deltaic mouth bars. In the Montllobat interval, these sediments comprise the Castigaleu Formation. In the Ainsa Basin, marine siliciclastic and carbonate slope facies are incised by deep, composite submarine canyon fills (Marzo *et al.*, 1988; Nijman, 1990; Ayckbourne *et al.*, 2024). Siliciclastic sediment was further routed through submarine channels into the distal Jaca Basin, which is dominated by Hecho Group turbidite deposits (Mutti, 1985a).

The Hecho Group (Fig. 3) is dominated by thick-bedded turbidites, interbedded with deep water mudstones and thin-bedded turbidites (Mutti, 1985b). Each turbidite system in the Jaca Basin (in stratigraphic order, the Pre-Torla, Torla, Broto, Cotefablo, Banastón, and Jaca turbidite systems; Fig. 3) represents between 500 and 1000 m of stratigraphy, and these successions are punctuated by 8 large-volume event beds, or Mega Turbidites (MTs; Seguret *et al.*, 1984; Labaume *et al.*, 1987; Remacha & Fernández, 2003), used to inform correlation frameworks. There is, however, some inconsistency amongst published correlation schemes

and stratigraphic frameworks for the Jaca Basin, and some schemes are directly contradictory (Scotchman *et al.*, 2015). In Figure 3 we present the stratigraphic framework selected for our primary intermittency analyses, based on a compilation of correlations (Remacha & Fernández, 2003; Payros *et al.*, 2009; Caja *et al.*, 2010; Scotchman *et al.*, 2015; Chanvry *et al.*, 2018). Alternatively, some schemes correlate the Castissent Formation to the Torla-Fosado units in the Ainsa-Jaca Basin, and the Montllobat Formation to the Pre-Torla turbidite system (Mutti, 1985b; Labaume et al., 1987; Gupta & Pickering, 2008; Garcés et al., 2020; Muñoz et al., 2025). In the Supplementary Materials (section S4) we discuss these differing correlation schemes in detail.

Different potential stratigraphic correlations somewhat alter depositional volume reconstructions associated with each successive fluvial system, meaning the correlation we use might result in minor differences in reconstructed sediment intermittency factors. However, these uncertainties do not impact the duration of each depositional interval. To avoid inconsistency, we have selected the correlation framework shown in Figure 3, based on a compilation of schemes (Remacha & Fernández, 2003; Payros *et al.*, 2009; Caja *et al.*, 2010; Scotchman *et al.*, 2015; Chanvry *et al.*, 2018), and chosen for simplicity to avoid potential disagreements in the exact correlations between the Tremp-Graus Basin, Ainsa Basin and the individual MTs in the Jaca Basin. Henceforth, we assume the Arro and Fosado Channels in the Ainsa Basin are correlated eastwards to the Castissent Formation in the Tremp-Graus Basin (Poyatos-More, 2014; Chanvry *et al.*, 2018) and westwards to the Torla and Broto turbidite systems in the Jaca Basin (Mutti, 1985b; Labaume *et al.*, 1987; Gupta & Pickering, 2008). Any Jaca Basin clastic sediment between the top of the Lower Eocene Alveolina Limestone and the base of the Torla turbidite system should be associated with the pre-Castissent fluvio-deltaic deposits of the Tremp-Graus-Àger Basin, including the Figols Group and Montllobat Formation (Remacha & Fernández, 2003). These intervals can be identified in the Jaca Basin as the Figols and Castigaleu turbidite systems (Caja *et al.*, 2010). The upper Montanyana Group is correlated to the later Jaca turbidite systems. Hence, the stratigraphic

correlation framework we prefer in our volumetric reconstructions is as follows: the Castissent Formation in the Tremp-Graus Basin correlates with the Fosado-Arro channels in the Ainsa Basin, and the Torla-Broto turbidite system in the Jaca Basin; the Montllobat and Castigaleu formations in the Tremp-Graus Basin correlate with the uppermost succession of the Pre-Torla turbidite system, also known as the Castigaleu turbidite system, in the Jaca Basin.

We note that this is not the only possible interpretation of the available stratigraphic frameworks linking the Tremp-Graus, Ainsa and Jaca basins (e.g., Fig. S2). In Section 5.2 we discuss the potential impacts of uncertainty in correlations on intermittency factor reconstructions, provide alternative I_s values, and conduct further analyses to corroborate the results.

Sediment thickness

To calculate depositional volumes along the source-to-sink correlations described above, we used a series of published outcrop measured sections, sedimentary logs and grain-size distribution estimates through the Eocene foreland basin (Fig. 4).

In the Tremp-Graus Basin, we estimated the thickness of sandstone and coarser sediment using 16 previously published measured sections (Tables S3, S4; Nijman, 1998; Chanvry *et al.*, 2018). To estimate the total apparent thickness of the units in the Jaca and Ainsa basins, we used geological maps resolving the Torla-Broto and Pre-Torla turbidite systems (IGME, 2003; Remacha & Fernández, 2003; Chanvry *et al.*, 2018) to measure the apparent thickness of these units based on the maximum topographic range of the mapped outcrop. In this topographic approach, we measured the Torla-Broto unit to represent Castissent-age sediment, and the Pre-Torla unit to represent Figols-to-Montllobat age sediment according to our correlation framework (Fig. 3). We outlined 15 km boxes oriented parallel to palaeocurrent direction along the mapped outcrop, determined based on sedimentological observations (Marzo *et al.*, 1988; Cornard & Pickering, 2020; McLeod *et al.*, 2025) and measured the maximum topographic range within the mapped outcrop for each turbidite system to attain an

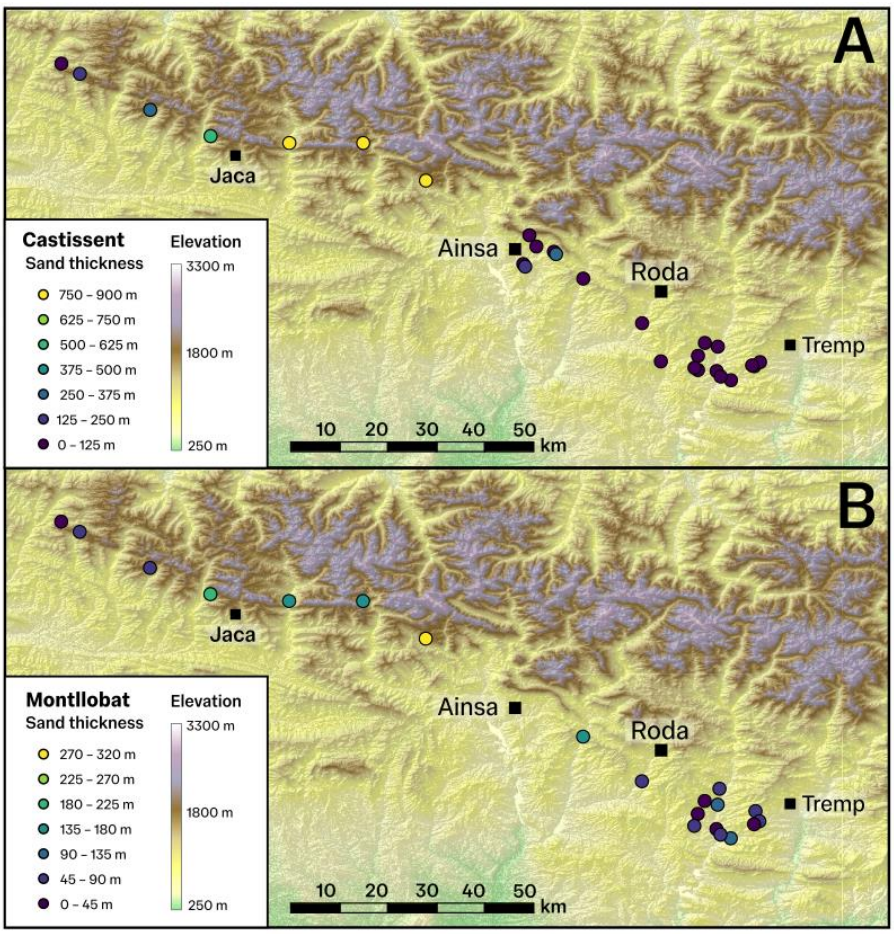

Figure 4. Sand thickness dataset locations for the (A) Castissent Formation and correlative strata (Fig. 3), and (B) Montllobat Formation and correlative strata (Fig. 3). Data points are coloured according to total sand deposit thickness. See Supplementary Material (section S2) for the full thickness dataset.

estimate of total unit thickness. This approach, used in the context of our stratigraphic framework, permits simple measurements of stratigraphic thickness. The thickness estimates yielded by our approach are reasonable, with maximum values of 375 – 1300 m: they present both a lower bound on thickness considering erosion that may have taken place following exhumation, and an upper bound on thickness considering structural thickening of the units due to compression.

To estimate sediment thickness in each member of the Castissent and Montllobat-age fluvial and shallow-marine deposits, we used published measured outcrop sections in the Tremp-Graus basin (Tables S3, S4; Nijman, 1998; Chanvry *et al.*, 2018) to estimate the average thickness ratio between the members within each formation. We extrapolated these thickness ratios across the Ainsa and Jaca basins, assuming that the thicker members and sequences

in the alluvial domain correspond to thicker deposits downsystem in the marine domain of this foreland basin. These approaches generate reasonable first-order estimates of stratigraphic thickness through the Ypresian Pyrenean foreland.

Sand proportion

We next required estimates of the proportion of each unit comprised of sandstone, as a counterpart to the bankfull sand transporting capacity we will calculate for the Castissent and Montllobat rivers.

We employed an approach using total sediment thickness measurements and estimates of sandstone proportion. According to the stratigraphic correlation framework used (Fig. 3) the Castissent rivers correlate to the Torla-Broto turbidite systems and the Montllobat rivers to the comparatively sand-poor Castigaleu turbidite system. In the continental Tremp-Graus Basin, a high density of measured sections (Nijman, 1998; Chanvry *et al.*, 2018) permitted direct measurements of sandstone proportion in the Castissent and Montllobat deposits at those locations. In the Ainsa and Jaca basins, there is more uncertainty associated with sandstone proportion within each unit.

To estimate sand proportion in the Castissent- and Montllobat-aged units of the Ainsa-Jaca basin, we first collated estimates of sandstone proportion across the basin. To obtain data support for estimates of the amount of sand entering the deep marine basin, we used measured sections from the Broto region for the Castigaleu turbidite system (Raimat Quintana *et al.*, 1997), and for Castissent-age sediment (Arro-Fosado deposits) in the Ainsa Basin we used measured sections from Ayckbourne *et al.* (2024) and Chanvry *et al.* (2018). To determine the proportion of the Pre-Torla sediment thickness that is attributed to the sandstones of the Castigaleu turbidite system, we used the measured sections of Caja *et al.* (2010). Based upon these estimates for the Broto region, where sand entered the deep marine basin, we estimated a linear down-system trend of decreasing sand content that is calibrated to measurements from the Broto turbidite system (Cornard & Pickering, 2020), which we

applied to both Castissent- and Montllobat-age deposits. We subsequently estimated sandstone thickness in the Jaca Basin by scaling our total unit thickness estimates from the topographic approach described above, according to the sandstone proportions acquired from the linear down-system fining trend. This approach permits the characterisation of sandstone thickness from source to sink (Figure 6; Tables S3, S4).

Volume calculation

To estimate the deposit volumes based on the above constraints on sand thickness, we first required estimates of sediment fairway geometry. To estimate the shape and size of the sediment fairway in the Jaca Basin, we used reconstructions of palaeogeography (Remacha *et al.*, 2005; Vinyoles *et al.*, 2021) and turbidite deposit extent based on the Broto turbidite system (Cornard & Pickering, 2020). In the Tremp-Graus, Àger and Ainsa basins, fairway extent was based on outcrop extent, palaeogeographic reconstructions (Juvany *et al.*, 2024) and structural controls including the positions of the Montsec and Boixols thrusts which imposed constraints on sediment routing. We accordingly allocated the edge of the sediment fairway zero sand thickness (Tables S3, S4). Thus, from outcrop sections, sedimentary logs and, grain-size distributions and palaeogeographical reconstructions, we resolved 1D sediment thicknesses across the early Eocene source to sink system.

Whilst folding and thrusting in the northern part of the Jaca basin (e.g., Muñoz *et al.*, 2025) modifies unit geometry and could therefore introduce uncertainty regarding true unit thickness, average bedding dip is <10˚ basin-wide, meaning that true unit thicknesses could be c. 2% less than their apparent thicknesses. This uncertainty is significantly less than those involved in estimating Jaca Basin sediment fairway geometry and stratigraphic correlation, so it is disregarded for further analysis, and we treat sediment thickness measurements as estimates of true unit thickness.

Using industry-standard subsurface mapping software, we applied a convergent interpolation method (Schlumberger, 2017) to interpolate our 1D sediment thickness dataset to a sediment

thickness grid for the full fairway. To address uncertainty in sediment thickness grids arising from the outcrop sections, logs, sandstone proportions and fairway geometries used, we produced two isochores for each time interval: one in which the maximum thickness of the unit was permitted to be 10% greater than the limit of input data, improving the smoothness of isochore surfaces and implied basin geometry; and one with a 0% leeway on the maximum unit thickness (Table S2). After manual smoothing, we then calculated the integrated volumes of the interpolated sediment thickness grids. These volumes were decompacted according to a sandstone decompaction factor, estimated as the ratio of compacted sandstone porosity (0.1-0.25) to original (depositional) sandstone porosity (0.4-0.5) (Fisher *et al.*, 1999; Kim & Lee, 2018), and a denudational weathering rate due to carbonate dissolution between 0 and 20% (Schoonejans *et al.*, 2016; Ott *et al.*, 2025; see Table S4 in the Supplementary Materials for a list of uncertainty bounds used in analysis).

3.2 Water and sediment fluxes and intermittency factors

Bankfull transport capacities

Our methodological approach for reconstructing bankfull water and sediment transport capacities in ancient rivers using palaeohydrology follows a workflow which has been tested in various geological settings (e.g., Ganti *et al.*, 2019; Lyster *et al.*, 2020; Wood *et al.*, 2022; McLeod *et al.*, 2025). To characterise river transport patterns in the Tremp-Graus Basin, we leverage the study of McLeod *et al.* (2025), which reconstructed the bankfull water and sediment transport capacities for the Montllobat and Castissent formations. Their dataset included a total of 1686 measurements of dune cross-set height, 221 barform accretion heights, 147 grain-size measurements, 856 measurements of palaeocurrent direction, 703 measurements of barform accretion orientation and 46 measurements of accretion length across 42 outcrops in the Spanish Pyrenees (19 in the Montllobat Formation and 23 in the Castissent Formation). These primary field observations were combined with previous facies analyses and stratigraphic correlations constrained by extensive outcrop mapping across the Tremp-Graus Basin (e.g., Marzo *et al.*, 1988; Nijman, 1998; Chanvry *et al.*, 2018; Honegger

449 *et al.*, 2020) to obtain sequence-scale (member-scale) estimates of evolving river morphology
450 and style, and landscape-scale water and sediment transport rates in the Ypresian.

451 Since the Jaca Basin was also supplied from the Àger Basin, we supplemented
452 palaeohydrological analyses of the Castissent and Montllobat formations with new estimates
453 for the Corçà Formation, the major river system active in the Àger Basin during the Ypresian.
454 For this, we used field observations to estimate channel geometry and slope, and used an
455 analytical workflow based on a suite of theoretical-numerical models, experimental relations
456 and field observations (c.f. McLeod et al., 2025) to reconstruct the bankfull transport capacities
457 of water and sediment through the Corçà river system. This approach is briefly described
458 below; further details are available in the Supplementary Materials (Section S1).

459 Cross-sets (Fig. 5B, E, H), the preserved remnants of river dunes, generally scale in size with
460 river flow depth (Bradley & Venditti, 2017), thus presenting an indicator of palaeo-flow depth.
461 To estimate mean cross-set thickness, h_{xs}, from fluvial deposits in the Corçà Formation, we
462 obtained full thickness distributions by measuring thickness along the major axis of a cross-
463 set at 10-15 regular intervals. Original dune height, h_d, was estimated using the relation of
464 Leclair & Bridge (2001) where mean cross-set thickness is, on average, around 1/3 of the
465 original dune height:

466 $$h_d = C h_{xs} , \quad (3)$$

467 and *C* is a bedform preservation ratio with a value of 2.9 ± 0.7, derived from observational
468 river datasets and flume experiments. The relation of Bradley & Venditti (2017) permits
469 estimates of median formative flow depth, *H*, from h_d:

470 $$H = x h_d , \quad (4)$$

471 where *x* is a scalar based on compiled observational flow and dune dimension data, with an
472 interquartile range between 4.4 and 10.1, and a median value of 6.7 (Bradley & Venditti, 2017).

The results of this approach were independently compared with the thickness of barform accretion sets (Fig. 5A, D, G), which represent minimum constraints on formative flow depth.

In each observed cross-set, we measured median grain-size (D_{50}) (Fig. 5C, F, I) and lee face orientation. Where grains were <2 mm in diameter, D_{50} was estimated using the scheme of Wentworth (1922), and in conglomeratic bodies with $D_{50} \geq 2$ mm, grain size distributions were measured according to the point-count method of Wolman (1954) with at least 100 observations, allowing reconstruction of maximum formative flow conditions according to average bedload material grade.

Estimates of D_{50} and H were used to reconstruct palaeo-channel gradient or slope, S, using the approach of Trampush *et al.* (2014). This method is based on empirical data rooted in hydrological theory and is appropriate for the range of grain-sizes observed in the Montllobat, Castissent and Corçà formations, including applications to suspended, mixed and bedload rivers. S (in units of m/m) is given by:

$$logS = \alpha_0 + \alpha_1 logD_{50} + \alpha_2 logH\,, \quad (5)$$

where α_0, α_1 and α_2 are constants given as −2.08±0.036, 0.254±0.016 and −1.09±0.044 respectively.

We estimated water flow velocity using the formula established by Manning *et al.* (1890), from which we used H estimates to reconstruct the per-unit-width water discharge, q_w. To reconstruct per-unit-width bankfull sediment transport capacity q_s, we used the total load predictor of Engelund & Hansen (1967) for sand-dominated deposits, and the bedload predictor of Meyer-Peter & Müller (1948) for gravel-dominated deposits (see Suppementary Material S1 for further details). To upscale q_s and q_w estimates to the bankfull transport capacity of ancient river channels, we estimate river width using scaling relations for low-sinuosity rivers (Long, 2021). This provides estimates of individual channel width (i.e. a single thread) based on values of H, and uncertainty is modelled using a rectangular distribution within the interquartile range of H. Rates of bankfull water and sediment discharge per

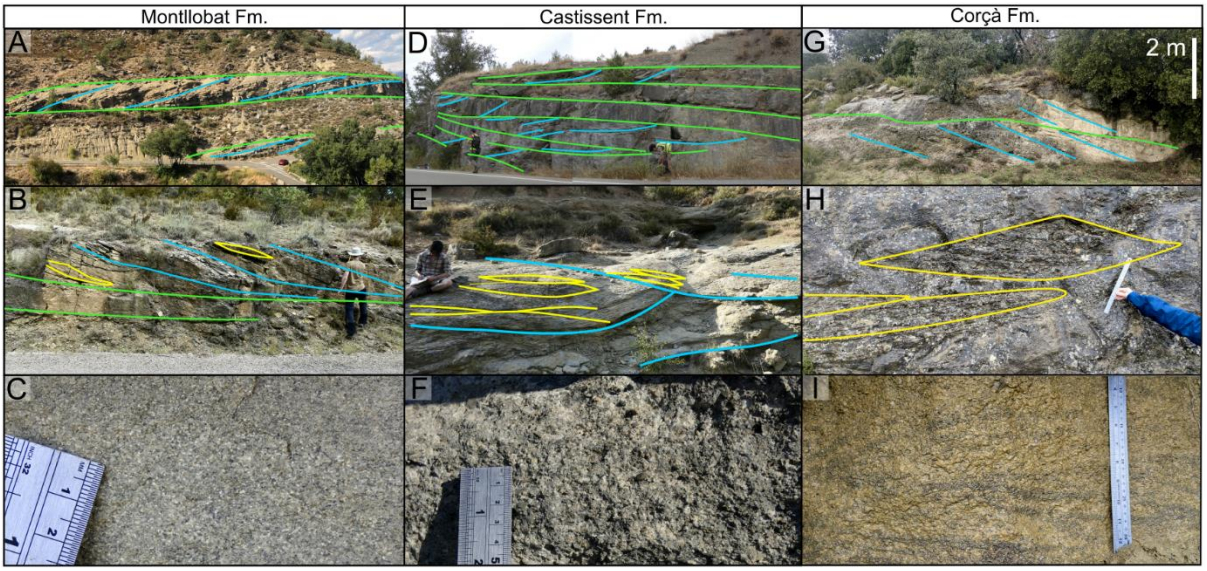

Figure 5. Exposures of the fluvial Montllobat, Castissent and Corçà formations at (A, D, G) channel scale; (B, E, H) bedform-scale; and (C, F, I) grain-scale. Coloured outlines highlight interpreted alluvial architectural features where green represents barform-bounding surfaces, blue represents barform-accretion surfaces and yellow represents dune-scale cross-set bounding surfaces. See Supplementary Material (Fig. S1) for an unannotated version.

channel, Q_w, (with units m^3/s) can be estimated according to $Q_w=q_wW$, where q_w is the discharge per unit width.

Finally, to obtain the total water and sediment discharge rates for a full river system, $Q_{s,w(total)}$, the number of threads in an ancient system must be estimated according to $Q_{total} = N_t Q$, where N_t is the average number of active river threads or channels. We used two approaches described in detail by McLeod *et al.* (2025) to determine the likely channel count, sinuosity and planform classification of the Montanyana rivers, and subsequently the total channel-forming water and sediment discharge in the Corçà rivers. This palaeohydrological workflow, using primary field observations and an analytical toolkit based on empirical relations grounded in hydrological theory and observations, provides a robust and tangible method of understanding landscape-scale water and sediment transport capacities through river channels.

Palaeo-routing scenarios

Despite well-constrained bankfull water and sediment transport capacities in the Montllobat and Castissent formations in the Tremp-Graus basin, there are uncertainties as to the source

514 regions of these river systems, their catchment areas in relation to those of the coeval Corçà
515 Formation in the Àger basin, and the size of their depositional sinks. Current palaeogeographic
516 and palaeohydrological reconstructions are not able to determine the relative transport
517 capacities and depositional contributions of palaeo-rivers in the Tremp-Graus basin versus the
518 Àger basin.

519 Based on palaeogeographic reconstructions (Martinius, 2012; Garcés *et al.*, 2020; Juvany *et*
520 *al.*, 2024), petrological analyses (Nijman, 1998; Clark *et al.*, 2017; Roigé *et al.*, 2026) and
521 palaeohydrological reconstructions (McLeod *et al.*, 2025), we identify two potential end-
522 member scenarios for the sediment routing systems of the Eocene foreland in the Ypresian,
523 considering uncertainties in the final depositional sink of the Corçà Formation and the
524 catchments of the Corçà, Montllobat and Castissent formations. We outline these scenarios
525 in Figure 6. In one scenario (Montllobat Scenario A), the petrographic differences between the
526 Corçà and Montllobat formations are used to infer that the two river systems had mostly
527 distinct, separate catchments, both feeding into the same turbiditic sediment volume in the
528 Jaca basin by an unknown route over the Boltaña Anticline. We may conversely treat the
529 Castissent and Corçà rivers as one system, to account for the petrographic similarities
530 between the two formations (Castissent Scenario A). This Castissent/Corçà axial system,
531 incorporating Àger and Tremp headwaters, might then have split either side of the Montsec
532 thrust before merging and feeding into the same Jaca Basin clastic sink (c.f. Martinius, 2012).

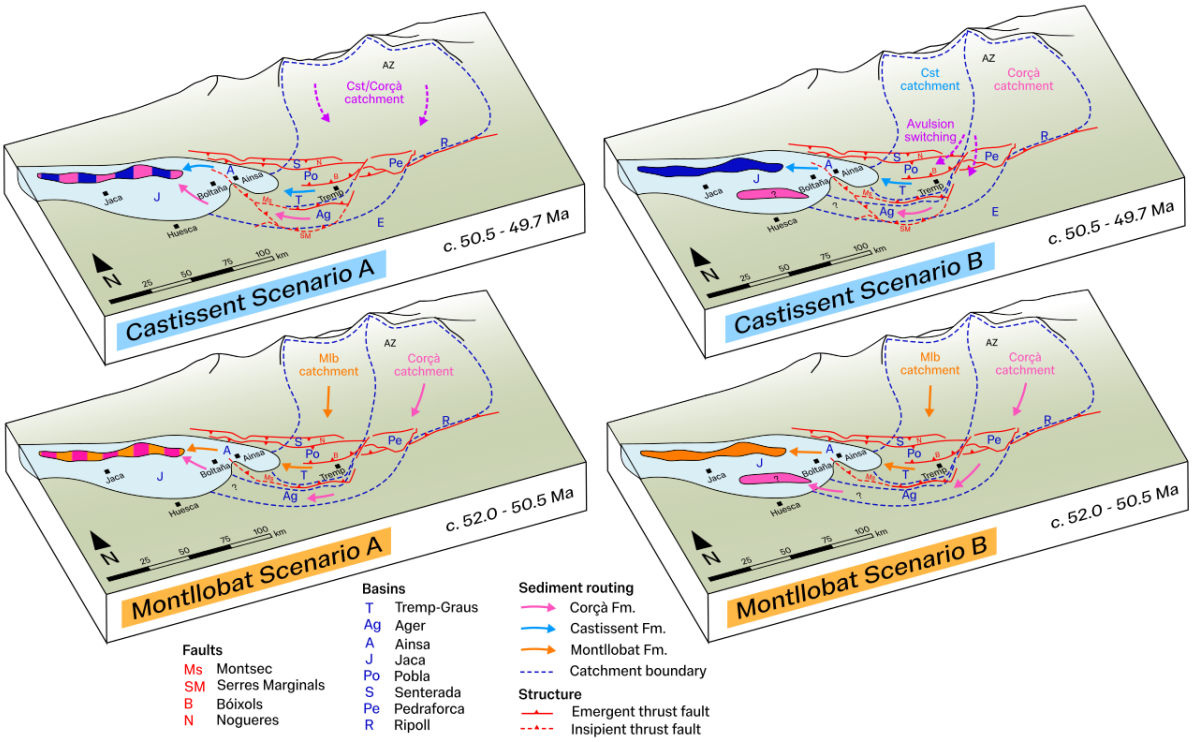

Figure 6. Palaeo-sediment routing scenarios for the Montllobat and Castissent intervals, highlighting two alternative scenarios for the source-to-sink palaeogeography of the Montllobat and Corçà rivers (Montllobat Scenarios A and B) and for the Castissent and Corçà rivers (Castissent Scenarios A and B) in the early Eocene south central unit of the Pyrenean foreland.

Another potential scenario (Montllobat Scenario B), arising from uncertainty as to the precise sources of the Hecho turbidite systems, is that the Montllobat and Corçà rivers contributed to two separate depositional sinks. Turbidite deposits associated with the Corçà rivers in the LM interval may have been located elsewhere in the Jaca Basin, for example more proximal to the Guara carbonates to the south of the basin, and/or these distal deposits are simply not exposed today. Likewise, the same may have been true of the depositional sinks in the Castissent interval (Castissent Scenario B). It is possible that, despite being two essentially separate river systems, there was increased fluvial connectivity between the Castissent and Corçà rivers across the Montsec thrust (Nijman, 1998), but ultimately the marine depositional sinks did not merge in the Jaca Basin. Equally, the Tremp-Graus (Castissent) and Àger (Corçà) branches of the rivers may not have been active at the same time: one possibility to explain the petrological and palaeogeographical features of the Montllobat, Castissent and Corçà routing systems is river switching by large-scale avulsion, with alternating phases of fluvial routing and deposition through the Àger Basin and the Tremp Basin. The Corçà river

system, which could have been mostly confined to the Àger Basin at c. 52-50.5 Ma could have intermittently avulsed into the Tremp-Graus basin from c. 50.5-49.7 Ma, producing the Castissent Formation. This would mean that the total transport capacity of the system would be no greater than that of the river branches in each individual sub-basin.

To account explicitly for these uncertainties in sediment routing during the Ypresian, we generated two intermittency scenarios for each time interval according to our Scenarios A and B outlined above (Fig. 4). For Montllobat Scenario A, we combined the bankfull sediment transport capacity of the Tremp-Graus Basin with that of the Àger Basin, acquired from the Corçà Formation. Likewise, for Castissent Scenario A, we combine the transport capacities of the Tremp-Graus and Àger basins, but we treat the catchment area for the Corçà and Castissent rivers as the same, meaning that the Casisstent Scenario A catchment area is double that of Montllobat Scenario A. In Montllobat and Castissent Scenario B, we assume the depositional volume of the Montllobat sink can be directly compared with the bankfull sediment transport capacity of the Tremp-Graus Basin, disregarding input from the Àger Basin. The results we present, therefore, are represented in these two end-member scenarios.

These palaeo-sediment routing scenarios bound the palaeogeographical unknowns in the lower Eocene. We combine these estimates of landscape-scale water and sediment transport capacities with long-term discharge rates, below, to calculate evolving intermittency factors for the Eocene Pyrenean foreland.

Mean sediment flux

To estimate long-term sediment flux from a decompacted depositional sandstone volume, estimates of the duration of deposition must be incorporated into analysis. Based on a compilation of age-date estimates (Bentham & Burbank, 1996; Nijman, 1998; Mochales *et al.*, 2012; Scotchman *et al.*, 2015; Westerhold *et al.*, 2017; Chanvry *et al.*, 2018), we determined that the duration of the Montllobat Fm is 1.3 ± 0.1 Myr, and the duration of the Castissent Formation is 0.9 ± 0.1 Myr. For higher-resolution analysis of evolving sediment transport

patterns, we also estimated the duration of the members of the two formations. Castissent A (Cs-1) had a duration of 0.30±0.03 Myr, and Castissent B&C (Cs-2) lasted 0.6±0.03 Myr (Nijman, 1998; Mochales *et al.*, 2012; Westerhold *et al.*, 2017; Chanvry *et al.*, 2018). Montllobat A had a duration between 0.6 and 1.0 Myr (Chanvry *et al.*, 2018) with a preferred estimate of 0.9 Myr (Bentham & Burbank, 1996), and Montllobat B had a duration between 0.3 and 0.6 Myr (Nijman, 1998) with a preferred estimate of 0.4 Myr (Westerhold *et al.*, 2017). Sand-grade depositional volumes were divided by these durations to obtain rates of deposition for the intervals of focus. See Table S2 for the bounds used in Monte Carlo simulations to address the uncertainties in duration.

In addition to our uncertainty analysis, we used two approaches to validate the results from this methodology. Firstly, we divided estimated catchment areas (see Section 3.3 below) by depositional volumes to estimate catchment averaged erosion rates for each time interval. This revealed erosion rates which were aligned with estimates of exhumation rates based on detrital zircon thermochronological data (Whitchurch *et al.*, 2011). Secondly, we compared our downstream approach to reconstructing long-term depositional fluxes with an upstream approach based on the BQART model, a global multiregressional empirical model which estimates suspended sediment load (Syvitski & Milliman, 2007). For this, Yan *et al.* (2025) presented BQART-derived estimates of long-term bedload flux in the southern Pyrenees based on similar catchments reconstructed from palaeo-digital elevation models (pDEMs) for the slightly later Bartonian stage. These provide a useful, if not necessarily direct, comparison for our stratigraphic volume-derived depositional flux estimates.

Mean water flux

We calculated long-term average water discharge rates based on estimates of catchment area and precipitation rates. The climate was semi-arid to sub-humid, and estimates of precipitation rates from geochemical analyses of palaeosols (Honegger *et al.*, 2020) reveal mean annual precipitation (MAP) rates of 376 mm/yr, increasing to as high as 754 mm/yr during carbon isotopic excursions (CIEs) associated with hyperthermal events. Since sedimentary palaeo-

600 precipitation estimates are sparse in Montllobat-aged strata, we use the estimates of
601 Honegger *et al.* (2020) from the Castissent Formation for both intervals investigated in this
602 study. Environmental interpretations (Boyrie *et al.*, 2025) of Montllobat-aged strata in the
603 northern Pyrenees confirm that the climate and palaeo-precipitation were likely not
604 significantly different from those of the Castissent interval.

605 These estimates of average precipitation rates were used to reconstruct mean runoff rates
606 within the palaeo-catchments of the Castissent and Montllobat rivers. Catchment areas were
607 primarily estimated based on Ypresian palaeogeographic constraints on sediment routing
608 (Juvany *et al.*, 2024). We estimate catchment areas averaging 10,000 km^2 for Montllobat
609 Scenarios A and B and Castissent Scenario B, and 20,000 km^2 for Castissent Scenario A (Fig.
610 4). Palaeo-Digital Elevation Models (pDEMs) for the later Bartonian Pyrenees (Yan *et al.*,
611 2025) confirm these estimates are reasonable for the Ypresian to within a factor of c. 2: the
612 primary fluvial catchment from that study supplying the Jaca Basin in the Bartonian (41.2–37.7
613 Ma), which corresponds roughly to the Bartonian counterpart of the Ypresian Montllobat and
614 Castissent catchments, had an estimated area of >7000 km^2. We propagated all uncertainties
615 in catchment areas and precipitation rates through the remaining analyses.

616 Using field-derived palaeohydrological estimates of bankfull water and sediment transport
617 capacities, estimates of basin volumetrics, and reconstructions of precipitation volumes, we
618 are able to estimate the intermittency factors of water and sediment transport in these ancient
619 river systems by finding the ratio of $Q_{s,w(avg)}$ to $Q_{s,w(bf)}$ for each unit.

620 **4. RESULTS**

621 **4.1 Sediment volumetrics**

622 Using published measured sections and palaeogeographic reconstructions to inform sediment
623 thickness maps, we reconstructed the depositional volumes of sand-grade sediment
624 associated with the Montllobat and Castissent river systems (Fig. 7). The total volume of sand
625 in strata correlated with the Montllobat Formation across the Tremp-Graus-Ainsa-Jaca basins

was 1.28±0.3x10^{11} m^3, or 128±30 km^3, where the stated uncertainty is derived from sediment thickness grid interpolation end-members (Fig. 7D, E). The decompacted Montllobat sand volume was 1.92±0.11 x10^{11} m^3, or 192±11 km^3. The estimated sand volumes associated with Montllobat members A and B were 5.26±0.4x10^{10} m^3 and 5.36±0.3 x10^{10} m^3, respectively; 7.88±0.5x10^{10} m^3 and 8.04±0.5x10^{10} m^3 once decompacted. These member-level sandstone volume estimates were acquired independently using the grid interpolation method described above, and within uncertainties they sum to the total unit volume.

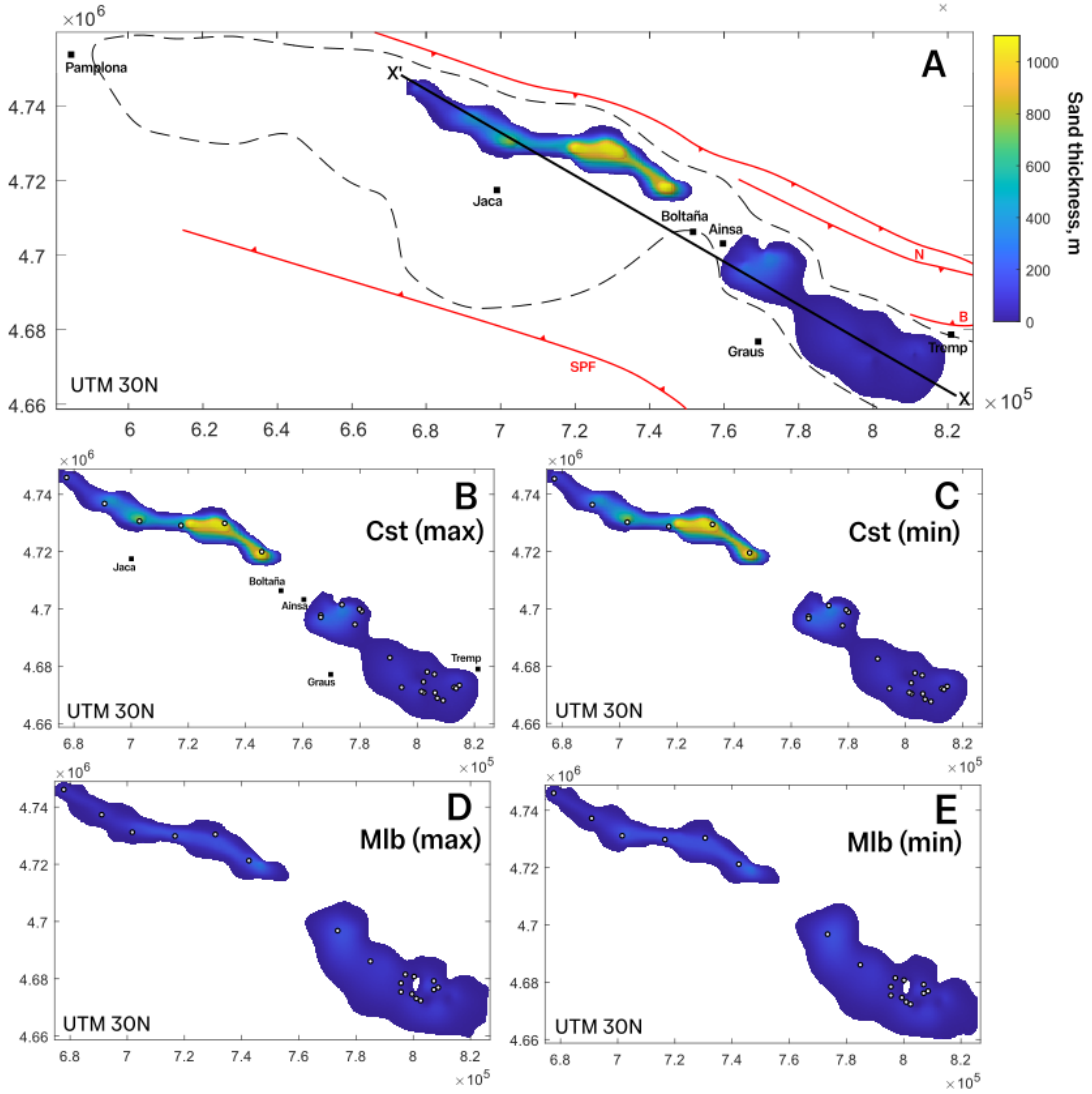

Figure 7. Sand volume isochores. (A) The structural and palaeogeographic context of the depositional sand volumes in the southern Pyrenean foreland superimposed on the minimum sand volume for Castissent-age strata (Fig. 7C), where the black line represents the palaeogeographic extent of the Tremp-Graus-Ainsa-Jaca basin (modified after Remacha et al. (2005)) and the red lines represent major thrust faults (N = Nogueres, B = Boixols, SPF = South Pyrenean Front). The volume is coloured according to total sand thickness. (B) The maximum and (C) minimum sand volumes for Castissent-age strata, where the white circles represent the thickness dataset. (D) The maximum and (E) minimum sand volume for the Montllobat-age strata. See Supplementary Materials (section S2) for sediment thickness data.

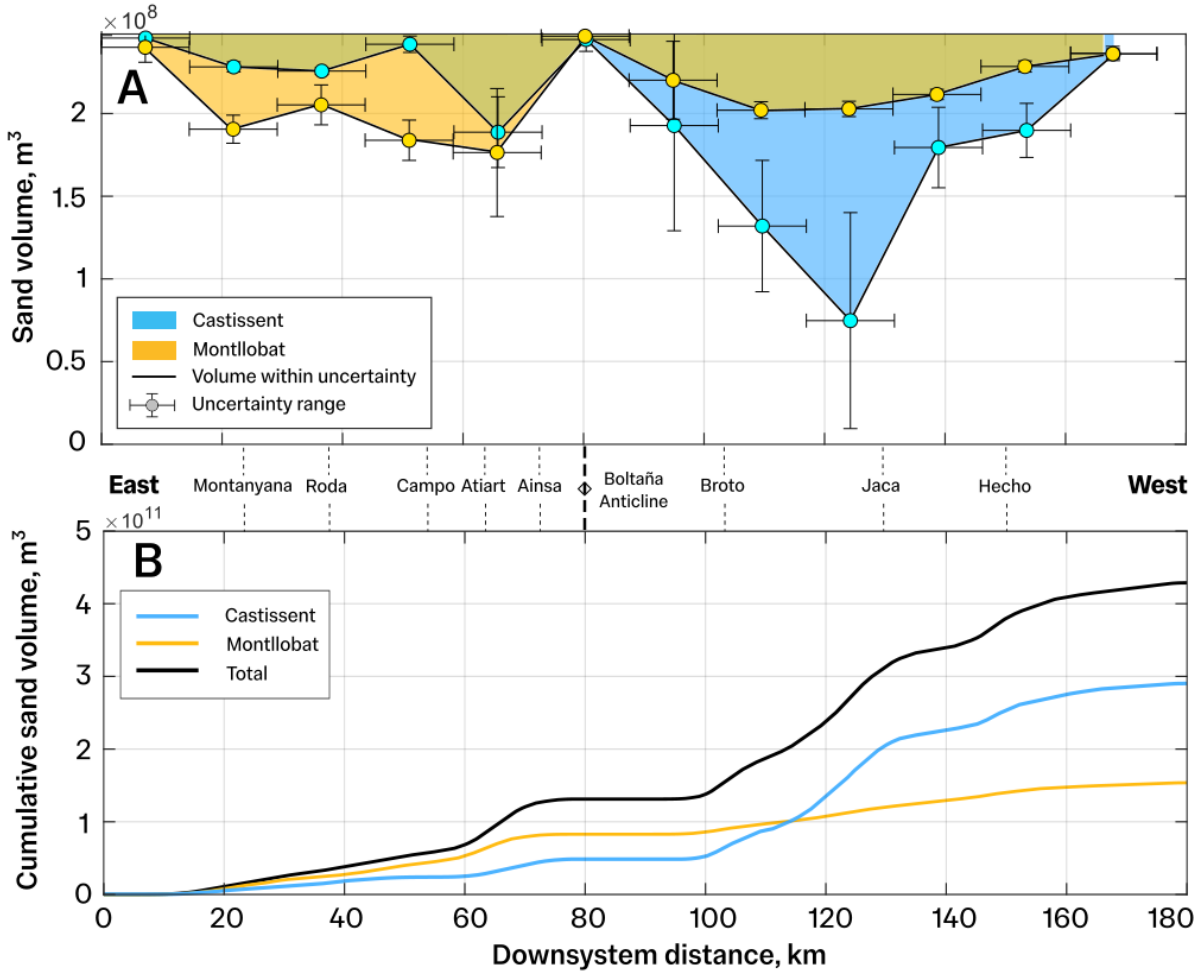

Figure 8. Downsystem sand-grade sediment volumetrics. (A) The sand volume along a downsystem transect (X-X' in Fig. 7A), where the Castissent-age volume is overlaid on the Montllobat volume. Uncertainty margins are based on the volume range within 15 km boxes along the transect, according to methodology for our topography approach (Methods). (B) The cumulative sand volume for each formation.

633 The total sand volume in Castissent-age strata was 2.92±0.1 x10^{11} m^3 (Fig. 7B, C), and
634 4.38±0.2x10^{11} m^3 after decompaction. For Castissent Member A the depositional sand volume
635 was 1.69±0.3 x10^{11} m^3, and for Castissent B&C it was 1.24±0.3 x10^{11} m^3. After decompaction,
636 Castissent Member A and members B&C had sand volumes of 2.53±0.1x10^{11} m^3 and
637 1.86±0.1x10^{11} m^3, respectively.

638 The down-system distribution of sand deposition is asymmetrical in both the Montllobat- and
639 Castissent-age strata (Fig. 8). In the continental deposits of the Tremp-Graus Basin, more
640 sand-grade deposition occurred in the Montllobat sediment routing system than in the
641 Castissent system (Fig. 8A). The Atiart canyon in the Ainsa Basin represents a significant
642 depositional sink of sand in Castissent-age strata, but in both units there is no sand volume

643 reconstructed over the Boltaña anticline, as discussed above. The Torla-Broto turbidite system
644 in the Jaca Basin preserves a greater sandstone volume than the Castigaleu turbidite system,
645 meaning that the cumulative Castissent-age sand volume is a factor of 2.3 greater than that
646 for the Montllobat-age system (Fig. 8B).

647 **4.2 Average water and sediment flux**

648 Employing estimates of the duration of each depositional interval derived from regional
649 chronostratigraphy (Bentham & Burbank, 1996; Nijman, 1998; Mochales *et al.*, 2012; Chanvry
650 *et al.*, 2018), we use these volumes to reconstruct sand deposition rates in the Eocene
651 Pyrenean foreland basin. Based on decompacted sediment volumes, the sand-grade
652 deposition rate in the Montllobat-age interval was 147±8 km^3/Myr, where the stated uncertainty
653 represents the interquartile range in the acquired results after Monte Carlo uncertainty
654 propagation. This represents the long-term mean sand flux in the Montllobat-age interval. In
655 strata equivalent to the Montllobat A Member, the mean sediment accumulation rate was
656 calculated as 94±9 km^3/Myr, and in strata equivalent to the Montllobat B Member, this rate
657 was 188±22 km^3/Myr. For the Castissent-age interval, deposition of sand-grade sediment
658 across the Tremp-Graus-Ainsa-Jaca basins averaged 487±30 km^3/Myr, three times greater
659 than that for the Montllobat-age interval. Mean sedimentation rate peaked in strata equivalent
660 to the Castissent A Member at 846±51 km^3/Myr. Strata equivalent to the Castissent B&C
661 members had a reconstructed depositional flux averaging 310±19 km^3/Myr.

662 As a check, we compared these reconstructed long-term averaged depositional fluxes to the
663 catchment areas estimated from palaeogeographic reconstructions, palaeo-DEMs and our
664 Scenarios A and B (Fig. 4). This enables calculation of the hinterland erosion rates that would
665 be required to supply the depositional sinks for each interval with sediment. In Scenario A for
666 the Castissent/Corçà system, we estimated a catchment area of 20,000 km^2, and in Scenario
667 B for this system, the catchment area is 10,000 km^2. We use a 10,000 km^2 estimated
668 catchment area in both scenarios for the Montllobat system (see Supplementary Table S4 for
669 full uncertainty ranges). Montllobat-age volumes imply sand-grade sediment was eroded from

Pyrenean catchments at rates of $1.1\pm0.3x10^{-2}$ mm/yr, and in the Castissent-age interval these rates increased to $3.6\pm1.0x10^{-2}$ mm/yr. These rates are reasonable considering rock uplift and exhumation rates reconstructed from thermochronological data (Whitchurch *et al.*, 2011; Curry *et al.*, 2021), (see section 5.2 for further details).

Average water discharges in the southern Pyrenean foreland were reconstructed based on published palaeo-preciptation rates (Honegger *et al.*, 2020) and estimated catchment areas. Average water discharge ($Q_{w(avg)}$) across the total catchment for both scenarios in the Montllobat-age interval was reconstructed as 68 ± 19 m^3/s, assuming a 20% evapotranspiration rate (Wang & Alimohammadi, 2012), where the stated uncertainty represents the interquartile range. $Q_{w(avg)}$ was also 68 ± 19 m^3/s in Castissent Scenario B, which used the same estimated values for precipitation rate and catchment area. However, in Castissent Scenario A, we assume a larger catchment area to incorporate Corçà headwaters. This yields an upper bound on average water discharge of 123 ± 42 m^3/s.

These long-term estimates of mean water and sediment flux permit a unique insight into the patterns of material transport through the Pyrenean foreland during the EECO. Using field-based observations of grain-, bedform- and channel-scale architecture, we compare these values to reconstructions of channel-forming (bankfull) conditions in these ancient river systems.

4.3 Bankfull water and sediment flux

Based on 42 field sites in the Tremp-Graus Basin, McLeod *et al.* (2025) reconstructed evolving river morphology and bankfull water and sediment discharge rates in the Montllobat and Castissent formations. These results are essential to our analyses, but the key to unlocking fully transport dynamics in the early Eocene is understanding the role of the Corçà Formation of the Àger Basin. Hence, we present new palaeohydrological results from the Corçà Formation (Fig. 9), in addition to briefly reiterating the key palaeohydrological characteristics of the Montllobat and Castissent formations.

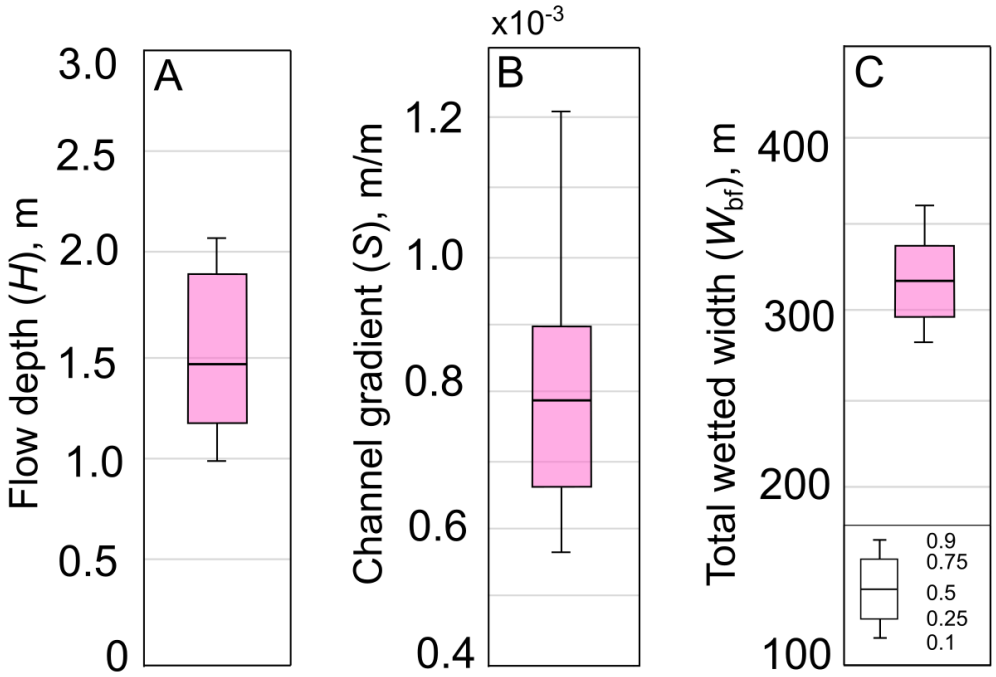

Figure 9. Corçà Formation palaeohydrology. (A) Bedform-derived palaeo-flow depth, (B) reconstructed palaeo-channel gradient, and (C) total flow width at bankfull.

The heights of bar accretion sets in the Corçà Formation averaged 1.48 m, providing a minimum channel-architectural constraint on palaeo-flow depth. By comparison, median barform-derived flow depths in the Montllobat and Castissent formations were both 1.40 m (McLeod *et al.*, 2025). This represents a conservative lower bound on flow depth because barforms are often not fully preserved in fluvial strata, and bars do not always accrete up to the bankfull flow depth. To support this analysis we used dune cross-set height scaling relations (Leclair & Bridge, 2001; Bradley & Venditti, 2017; Equations 3 and 4) to estimate the formative flow depth. This approach yielded flow depths (H) of 1.47±0.3 m, where the stated uncertainty represents the interquartile range, demonstrating these two approaches can be used to accurately predict palaeo-flow depth (Fig. 9A). Dune-derived palaeo-flow depths averaged 1.36±0.3 m in the Montllobat Formation and 1.26±0.3 m in the Castissent Formation (McLeod *et al.*, 2025).

Using our flow depth reconstructions and grain-size observations, we estimated channel palaeo-gradient or slope, S (Trampush *et al.*, 2014; Equation 5). Palaeoslopes in the Corçà rivers averaged $7.9\pm0.8\times10^{-4}$ (Fig. 9B), comparable with those of the Montllobat Formation which had S values of $8.0\pm1.5\times10^{-4}$, but the Castissent rivers had steeper channel gradients,

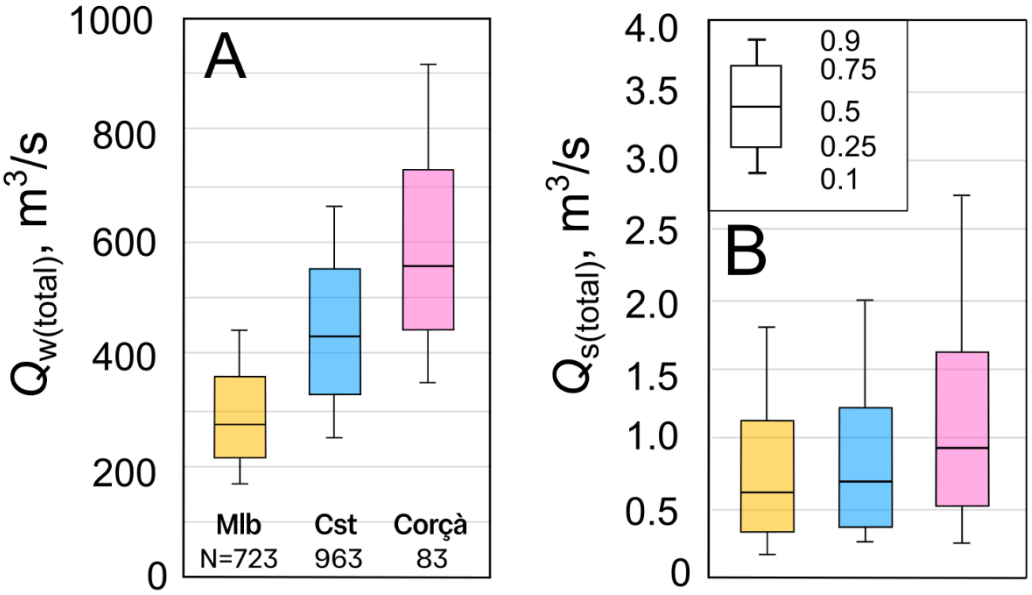

Figure 10. River discharge in the Tremp-Graus and Àger basins. (A) Total water discharge, and (B) total sediment discharge in the Montllobat (yellow), Castissent (blue) and Corçà (pink) formations.

averaging 1.2±0.3x10^{-3} (McLeod *et al.*, 2025). Based on depth-scaling relations (Long, 2021; Equation S8) the average bankfull channel width was estimated as 49±12 m, and considering palaeo-planform analyses (McLeod *et al.*, 2025), we reconstruct the total wetted width of the Corçà rivers as 318 m (Fig. 9C), compared to 225 m for the Castissent Rivers and 205 m for the Montllobat rivers (McLeod *et al.*, 2025).

Combining estimates of slope, depth and river width, total bankfull water discharge across the Corçà river system was reconstructed as 560±144 m^3/s (Fig. 10A), compared to 420±115 m^3/s in the Castissent rivers and 280±75 m^3/s in the Montllobat rivers (McLeod *et al.*, 2025). Total bankfull sediment flux was estimated to have been 0.91±0.59 m^3/s in the Corçà river system (Fig. 10B), 0.64±0.40 m^3/s in the Montllobat rivers and 0.68±0.41 m^3/s in the Castissent rivers (McLeod *et al.*, 2025).

4.4 Intermittency factors

We have reconstructed both average and bankfull water and sediment transport conditions in the river systems of the Àger and Tremp-Graus basins in the early Eocene, including formation- and member-level constraints on water and sediment discharge in the Montllobat and Castissent formations. The ratio of average to bankfull conditions describes the river

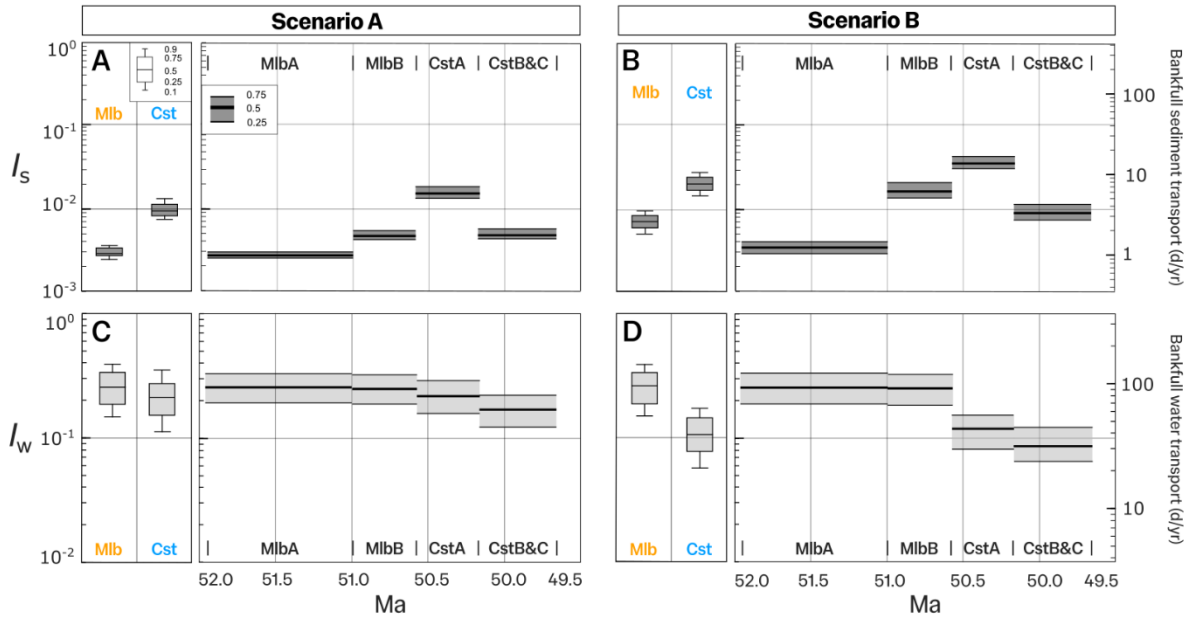

Figure 11. Evolving intermittency factors through time. (A) Sediment intermittency factors reconstructed using palaeo-routing Scenario A (Fig. 4), where boxplots represent average intermittency factors in the Montllobat and Castissent formations, and the evolution chart illustrates the changing I_s through time between members of the Montllobat and Castissent formations (x-axis). (B) Corresponding sediment intermittency factors reconstructed using palaeo-routing Scenario B (Fig. 4). (C, D) Water intermittency factors reconstructed using (C) palaeo-routing Scenario A and (D) palaeo-routing Scenario B (Fig. 4).

intermittency (I), or the fraction of time a river would require to transport its long-term water or sediment load if maximum transport conditions were sustained. We have investigated the uncertainties associated with depositional volume, catchment area and sediment routing pathways, and account for these uncertainties with two end-member scenarios A and B for the Montllobat-age and Castissent-age intervals (Fig. 4) which encompass the possible results (Fig. 11).

Water intermittency factors (I_w) in Montllobat-age rivers averaged 0.25±0.13 in scenarios A and B (Fig. 11C, D). In other words, considering the long-term water hydrograph of the river system, the average water discharge was 25% of the water discharge that carried out the majority of channel-forming work, likely representing bankfull conditions. This requires conditions in which around 3 months of sustained bankfull conditions would theoretically be required to complete the annual water budget. Castissent-age rivers had lower I_w values of 0.21±0.11 in scenario A (Fig. 11C) and 0.10±0.05 in scenario B (Fig. 11D), meaning average water discharges were 10-21% of potential bankfull rates. This means annual water budgets would be completed in 5-10 weeks if bankfull flow was to be sustained. Two-tailed KS tests

743 demonstrate that there is a statistically significant difference between I_w distributions in the
744 Montllobat Formation and the Castissent Formation ($p<10^{-3}$).

745 Sediment intermittency factors (I_s) in all cases are lower than I_w values, reflecting the
746 thresholded nature of sediment transport in rivers. The Montllobat rivers had I_s values
747 averaging $3.7\pm1.9\times10^{-3}$ in scenario A (Fig. 11A): the average sediment flux was 0.37% of the
748 maximum transport capacity at bankfull conditions. This means that, if the Montllobat river
749 system sustained bankfull conditions, the annual sediment load could be completed in as little
750 as 1 day. In scenario B, I_s was slightly higher at $6.7\pm1.2\times10^{-3}$, corresponding to 2.5 days of
751 bankfull conditions required to complete the annual sediment load (Fig. 11B). These
752 intermittency values suggest significant sediment transported occurred infrequently,
753 potentially during extreme events which surpassed sediment transport thresholds. Yet in both
754 scenarios, I_s was greater in Castissent-age rivers than Montllobat rivers, despite the fact that
755 the Castissent system had lower I_w value: I_s is $7.0\pm0.6\times10^{-3}$ in scenario A (Fig. 11A), and
756 $2.0\pm0.3\times10^{-2}$ in scenario B (Fig. 11B), meaning average sediment transport fluxes were 0.7-
757 2.0% of bankfull rates, corresponding to around 3-8 days of bankfull transport. Significant
758 sediment transport occurred more often in the Castissent-age interval than the previous
759 Montllobat-age interval. Member-specific I_s estimates show intermittency factors reached
760 maximum values in Castissent A rivers. Two-tailed KS tests demonstrate that there is a

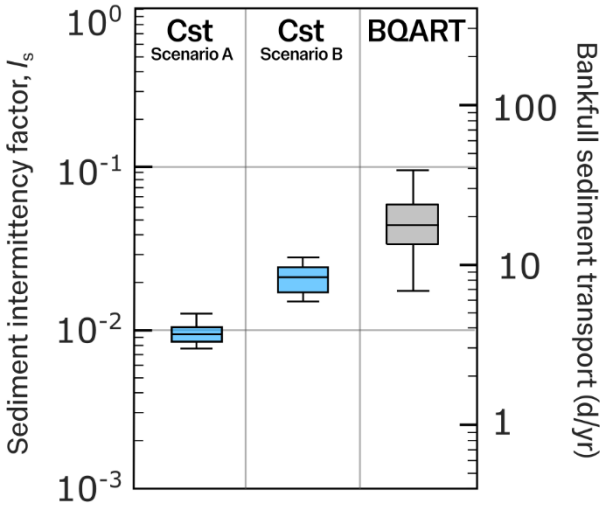

Figure 12. Comparison between sediment intermittency factors estimated for Castissent rivers using our approach outlined, and estimates from a BQART-derived equivalent.

761 statistically significant difference between the distributions of I_s in the Montllobat Formation
762 and the Castissent Formation ($p<10^{-3}$) for both scenarios.

763 We checked these sediment intermittency results from our downstream approach against an
764 alternative upstream approach. We used BQART-derived estimates of long-term bedload
765 sediment flux in the Bartonian, at c. 40 Ma (Yan *et al.*, 2025), and our estimates of $Q_{s(bf)}$ for the
766 Castissent-age interval as an illustrative example (Fig. 12). This provides an independent
767 estimate of I_s based on palaeo-catchment and climate characteristics, albeit for a later time
768 time interval than our Castissent-age data. Nonetheless, this test yielded I_s values of
769 $4.4\pm1.3\times10^{-2}$, which within uncertainty is of a similar magnitude to the estimate we derive from
770 our downstream approach, suggesting our field-based analyses produce reasonable results.

771 **5 DISCUSSION**

772 **5.1 Comparison with modern systems**

773 We reconstructed water intermittency factors (I_w) in the Montllobat Formation of 0.25, and
774 0.15-0.21 in the overlying Castissent Formation, meaning that annual water budgets could
775 have been completed in 2-3 months (15% - 25% of the year) if bankfull conditions were
776 sustained for that period. Practically, rivers with $I_w > 1$ are considered to be non-intermittent,
777 (Hedman & Osterkamp, 1982) containing water year-round. Sediment intermittency factors of

3-7x10^{-3} in the Montllobat Formation increased 3-fold to 1-2x10^{-2} in the Castissent Formation. This means the Montanayana river systems theoretically would have required as little as 1 day to transport their annual sediment load from 52.0-50.5 Ma, but the Castissent river systems required at least 3-8 days to achieve this result from 50.5-49.7 Ma. These reconstructed intermittency factors provide quantitative constraints on water and sediment transport patterns in the ancient river systems of the Eocene Pyrenean foreland for the first time. However, interpretations of environmental conditions in the lower Eocene are limited without comparison to intermittency factors in modern systems. Recent data describing present-day water and sediment intermittency on a global scale (McLeod *et al.*, 2026) make it possible to contextualise Montllobat and Castissent river activity with modern systems.

We compared our intermittency results from the Montllobat and Castissent formations to 297 modern river reaches with both I_w and I_s values across all continents, climate zones, and river planforms (Fig. 13) taken from McLeod et al. (2026). It is known that there is significant variability in intermittency factors worldwide, especially for sediment transport (Hayden *et al.*, 2021; McLeod *et al.*, 2026). For example, river reaches with the same I_w could display a 4 order-of-magnitude variation in I_s (Fig. 13). The water and sediment intermittency factors of the Montanyana Group rivers all plot within the range of these modern bounds, however, suggesting that water and sediment transport patterns in these ancient systems can be compared with modern analogues, with I_w and I_s values largely most similar to today's arid systems (Fig. 13).

We can illustrate this clearly on a cumulative curve of intermittency factors (Fig. 14A). Water intermittency factors averaging 0.25 in the Montllobat river system broadly lie at the median value (approximately 0.5 on the cumulative probability function) in comparison to the global dataset (McLeod *et al.*, 2026) across all river planform types, from braided to meandering. To provide examples of rivers with comparable water discharge patterns, the Montllobat river system had I_w values similar to the Kabul River in Afghanistan and the Zambezi River in Mozambique, both characterised by seasonal water discharge regimes. The Castissent river

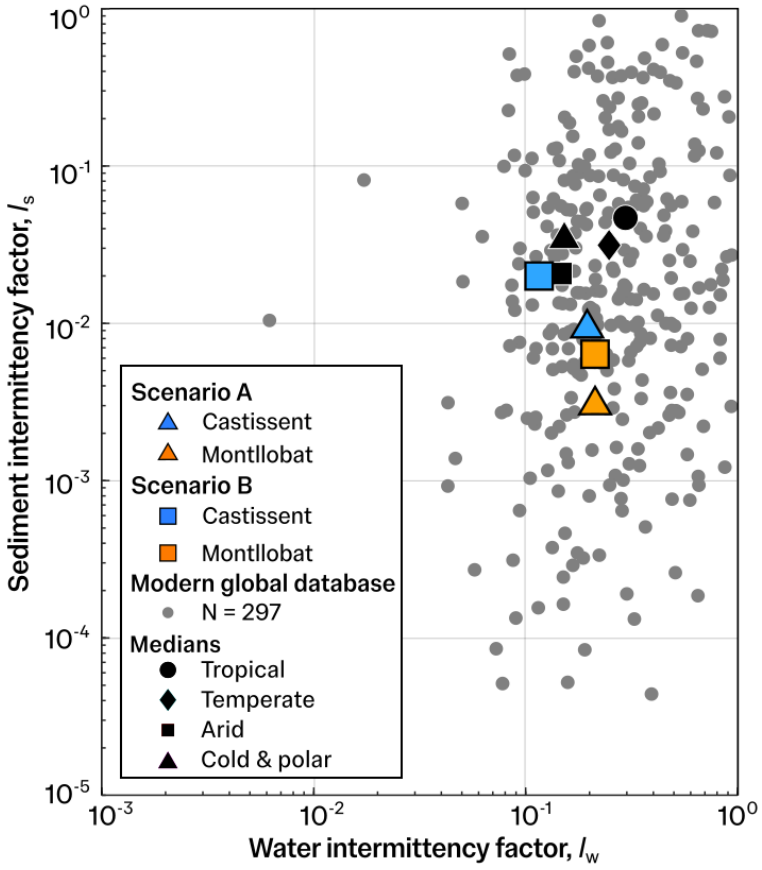

Figure 13. Comparison of intermittency factors for Montllobat and Castissent rivers with those for a global dataset of modern rivers (McLeod *et al.*, 2026).

system had somewhat lower I_w, plotting in the more ephemeral half of river reaches today, indicative of more intermittent (less perennial) water discharge conditions. Sediment intermittency factors were lower than average in the Montllobat and Castissent rivers compared to modern analogues: they transported sediment more often than the 15% most ephemeral systems but less often than the 55% most perennial rivers (Fig. 14A).

Planform reconstructions of the ancient Montanyana river systems, however, permit more detailed analysis of river sediment transport dynamics. Considering palaeohydrological and facies analyses, which demonstrate that the Castissent rivers were most likely braided (Marzo *et al.*, 1988; Nijman, 1998; McLeod *et al.*, 2025), we compare Castissent intermittency factors to modern braided rivers (Fig. 14B). This analysis reveals that sediment intermittency factors were relatively high in the Castissent rivers compared to a dataset of braided rivers across all climates today. Water intermittency factors, on the other hand, were in the lower 50% of the cumulative probability function, more ephemeral on average than the braided Kabul River.

This shows that the Castissent system transported sediment more perennially than most modern braided rivers, yet had a more intermittent water discharge regime than typical braided rivers today.

Montllobat rivers had meandering and multi-threaded reaches, and are interpreted to have had a wandering planform (McLeod *et al.*, 2025). Therefore, we also compared intermittency factors in modern wandering rivers to those reconstructed for the Montllobat system (Fig. 14C). Similarly to the Castissent rivers and their modern braided analogue (Fig. 14B), the Montllobat system had I_w comparable to the median of modern wandering river reaches across all climate zones, but higher than average I_s, meaning sediment export occurred more frequently than in most rivers with a similar planform today.

The Montanyana rivers also therefore differed with respect to most modern rivers: they transported sediment with higher I_s than the majority of modern systems with similar planform, size and aridity. Temperatures and precipitation rates can impose important bounding conditions on river activity, and potentially determine sediment export timescales and transport efficiency. The EECO represents a hothouse climate state that does not exist on Earth today, with MATs 8-15°C higher than today in what would be considered semi-arid conditions in modern climates. In order to explore the potential role of climate drivers and sediment supply in determining the unique transport patterns of both the Montllobat and Castissent rivers (Section 5.4), we first discuss the uncertainties in our analysis (Section 5.2) and then the implications of stratigraphic preservation (Section 5.3).

5.2 Impact of uncertainties

We have conducted a rigorous palaeohydrological analysis based on sediment volumetrics and field observations, and have accounted for uncertainty in our results using Monte Carlo simulations, as outlined in the Methods section. We now outline the impact of uncertainties on our key results. We used a stratigraphic framework based on a compilation of correlations (Remacha & Fernández, 2003; Payros *et al.*, 2009; Caja *et al.*, 2010; Scotchman *et al.*, 2015;

Chanvry *et al.*, 2018), selected for simplicity and consistency (Fig. 3). Alternatively, some schemes correlate the Castissent Formation to the Torla-Fosado units in the Ainsa-Jaca Basin, and the Montllobat Formation to Pre-Torla TS, and we present this scheme in the Supplementary Materials (Fig. S2).

We assess the impact of using an alternative stratigraphic framework on our intermittency results (see Supplementary Material section S4 for an extended explanation). If we assume the Ainsa-Jaca depositional volumes represent the total sand sink and the sand proportion in the Torla turbidite system is comparable to that of the Broto turbidite system, a competing stratigraphic framework (e.g., Mutti, 1985c; Labaume *et al.*, 1987; Gupta & Pickering, 2008; Garcés *et al.*, 2020; Muñoz *et al.*, 2025) would reduce decompacted sedimentation rate in the Castissent-age units by 50%, and consequently reconstructed I_s in the Castissent rivers would halve, from 0.009-0.020 to 0.005-0.010. The decompacted sandstone volume of the Montllobat Formation could be interpreted to correlate to the total volume of the clastic sediment beneath the Torla TS. The reconstructed I_s for the Montllobat Formation using this alternative correlation framework and subsequent estimates would increase from 0.0029-0.0067 to 0.0033-0.0076, an increase of up to 13%. Consequently, we conclude that our intermittency factors are robust in terms of order-of-magnitude trends.

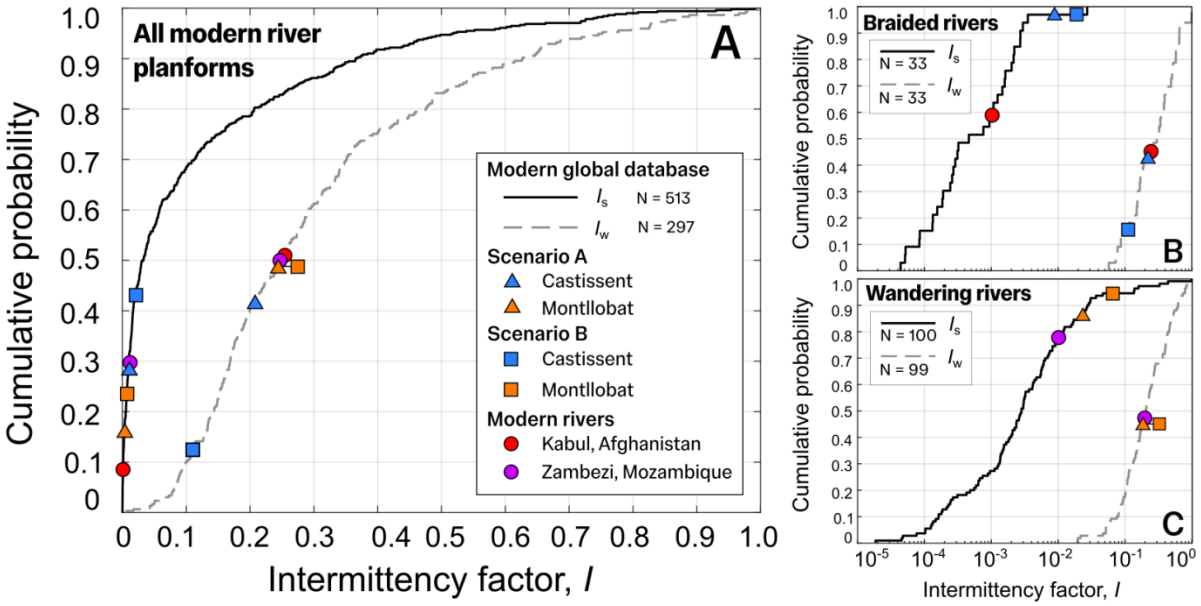

Figure 14. Cumulative probability functions of intermittency factors for a global compilation of modern rivers (McLeod *et al.*, 2026). (A) The cumulative probability functions of I_w and I_s for modern rivers of all planform types, with intermittency factor values for the Eocene Montllobat and Castissent rivers superimposed. (B) The cumulative probability function for modern braided rivers, with intermittency factors for Castissent rivers shown for comparison. (C) The cumulative probability function for modern wandering rivers, with intermittency factors for Montllobat rivers superimposed.

We interpreted a 3-fold increase in I_s at the onset of Castissent sedimentation. Using an alternative correlation framework which could yield greater Montllobat-age depositional volumes and smaller Castissent-age depositional volumes, this would be modified to a minimum 1.5-fold increase in I_s at the onset of Castissent sedimentation. Whilst there is a degree of uncertainty associated with stratigraphic correlations in this setting, this uncertainty would only change the I_s results by a factor of up to 2. Therefore, we suggest that sediment transport patterns likely changed at 50.5 Ma regardless of specific stratigraphic correlations in the Jaca Basin.

To provide additional corroboration of our original intermittency results beyond our Monte Carlo uncertainty analysis and considerations of stratigraphic correlation, we conducted further upstream-focused analyses to complement our primarily downstream-focused approach.

We estimated long-term sediment fluxes in the southern Pyrenean Foreland by calculating sand-grade depositional volumes along the sediment-routing fairway. As outlined in the Results, we compared the long-term sediment fluxes acquired from this volumetric approach

to sediment fluxes acquired from BQART-derived reconstructions of mean bedload sediment flux (Fig. 12; Yan *et al.*, 2025). The volumetrics derived from the BQART analysis correlate with those from our depositional approach, but reconstruct I_s values that are marginally higher than those reconstructed for the Castissent Formation (Fig. 11), suggest that reconstructed basin volumes may be slightly underestimated. On the other hand, we also corroborated our volumetric calculations by estimating catchment-averaged palaeo-erosion rates. By distributing the compacted sandstone volumes across our reconstructed catchment areas, we were able to estimate a lower-bound on erosion rates of $1.1\pm0.2\text{x}10^{-2}$ mm/yr in the Montllobat-age interval and $2.0\pm0.3\text{x}10^{-2}$ mm/yr in the Castissent-age interval. Accounting for average ratios of bedload to suspended load in the depositional sink of c. 0.1, based on our compilation of published stratigraphic sections (Supplementary Material section S2), these erosion rate estimates, to a first-order, align with rock uplift and exhumation rates reconstructed from thermochronological data of c. 0.2-0.8 mm/yr (Curry *et al.*, 2021), including a reconstructed increase in exhumation rate at c. 50 Ma. This alignment implies that we have estimated reasonable values of sand volume deposited in the southern Pyrenean foreland.

Our field-based approach and analytical workflow reconstruct ancient intermittency factors to a reasonable degree of accuracy, as corroborated by comparison with independent, upstream- and downstream-focused methods. Having established sediment intermittency factors in this ancient setting, we now discuss the implications of our results for the preservation of geological time.

5.3 Intermittency and stratigraphic preservation

Our recovered sediment intermittency factors, between $3\text{x}10^{-3}$ and $2\text{x}10^{-2}$, show the Montanyana rivers had an average sediment flux that was between 0.3% and 2% of potential instantaneous bankfull rates. It also suggests that the rivers were not actively moving sediment all the time. Considering the long-term hydrograph implied by these intermittency factors, one theoretical end-member for a low I_s could involve significant bankfull-capacity sediment transport occurring infrequently, only during extreme discharge events that surpass sediment

transport thresholds, with negligible sediment transport in-between those events. However, the stratigraphic record in the Montanyana Group and globally is not dominated by extreme events: most fluvial stratigraphy is not dominated by supercritical bedforms and other indicators of extreme activity. Rather, fluvial stratigraphy mostly preserves signatures of "ordinary" sediment transport (Sambrook Smith *et al.*, 2010; Paola *et al.*, 2018). Another theoretical end-member would involve the long-term sediment hydrograph distributed such that low sediment transport rates occur most of the time (e.g., Fig. 1B), which could support the observation of dominantly sub-critical or ordinary river sedimentation. Modern geomorphic observations suggest the more likely state of the long-term sediment hydrograph is somewhere between these two end-members, since geomorphic theory shows channel morphologies are self-organised such that sand-transporting conditions are surpassed close to bankfull water discharge rates, rather than only in extreme floods or in small amounts year-round (Phillips & Jerolmack, 2019). Significant sediment transport occurs during bankfull discharge events and floods, but these events do not have to be extreme.

The logical extension of this notion is that the Montllobat and Castissent formations preserve mostly ordinary time when sediment transport thresholds were surpassed, allowing dunes to migrate downstream when local aggradation and progradation cause local stratigraphic preservation. However, the direct implication of our reconstructed intermittency factors is that rivers were moving sediment a small proportion of the total time interval represented in stratigraphy, potentially as low as 0.3-2%, totalling only 7.5-50 kyr of the 2.5 Myr studied interval.

This is a common observation in sedimentary successions (e.g., Sadler, 1981; Paola *et al.*, 2018; McLeod *et al.*, 2023), and Paola *et al.* (2018) summarised this with the axiomatic notion that the overall low completeness of stratigraphy is caused by spatial and temporal intermittency of sediment transport and interaction. Spatial variability in alluvial settings causing local stratigraphic incompleteness can be viewed as variability in the spatial location of the river within the basin. Locally, the stratigraphic record may be incomplete as one

relatively brief phase of deposition is represented at outcrop, but the river will subsequently have migrated elsewhere and caused deposition in a different part of the basin. Over geological timescales it is to be assumed that every part of the basin will be visited by the river such that overall aggradation meets accommodation.

The other driver of stratigraphic incompleteness, temporal intermittency, can manifest at a range of timescales and could arise due to autogenic or allogenic processes. Autogenic or internal causes of temporal intermittency, and therefore local stratigraphic incompleteness, include enhanced bedform preservation as a consequence of morphodynamic hierarchy (Miall, 2015; Paola, 2016), and planform morphology which has been shown to change sediment transport thresholds (McLeod *et al.*, 2026). Allogenic or external causes include climate and tectonic forcing, which can affect stasis periods, subsidence rates, and sediment generation and mobilisation (Paola *et al.*, 2018). Paola *et al.* (2018) suggest that at sub-basin spatial scales (smaller than the sediment routing system of interest), allogenic forcings are unlikely to explain most signals of stratigraphic completeness, and that autogenic factors are the best way to frame investigations into the preservation of geological time (Muto *et al.*, 2007).

Our analysis, on the other hand, has reconstructed sediment volumetrics and dynamics at the basin scale: we measured the stratigraphic volume of two units from the most proximal to the most distal occurrence of sand-grade sediment in the basin. Erosion and lack of exposure means that this may not represent the full sand fraction within the lower Eocene Foreland Basin of the Southern Pyrenees, but as we have shown above through checks that use upstream- and downstream-focused approaches, it is a reasonable approximation. This means we are able to consider sand-transporting conditions from source to sink, at the scale of a full sedimentary basin. One significant benefit of this approach is that, by measuring deposition across an entire basin, our observations contain all spatial variability in aggradation and therefore can be considered to fully account for spatial intermittency, as discussed by Paola *et al.* (2018).

Despite a spatially complete record of sand grade sedimentation, our low reconstructed I_s values show clearly that geological time is not preserved completely in the alluvial part of this basin. Therefore, we must turn to temporal incompleteness and the final remaining cause of low stratigraphic completeness: temporal intermittency. Because we are dealing with broadly full spatial preservation, our sediment intermittency factors should map closely onto the proportion of time preserved in stratigraphy, and temporal intermittency must in this case be due to allogenic forcing. For example, the reconstructed increase in I_s at the base of the Castissent interval must indicate an increase in stratigraphic completeness, and be attributed to an allogenic driver. We note that in our approach, I_s is measured over the geologically short timescales represented by dune- and barform-scale cross-strata in channel-fill deposits, and it is measured and compared consistently on these deposits (and their implied durations). Consequently, our analysis is not biased by the 'Sadler effect' arising from interpretation of sedimentation rates across varying temporal scales (Sadler, 1981).

Paola *et al.* (2018) suggest variable external forcing is not necessarily important for regulating time completeness at sub-basin scales. We are suggesting that, given the spatial scale and temporal consistency of our study, we are able to assert that external forcing due to climate and tectonics is the most likely cause for a change in stratigraphic completeness that we infer at 50.5 Ma. Having established this, we are able to make important interpretations of the climate and tectonic state of the lower Eocene, and specific allogenic drivers that occurred at 50.5 Ma.

5.4 Eocene climate change in the Pyrenees

Our reconstructed intermittency factors in the Montllobat and Castissent formations permit interpretations of allogenic forcings in the lower Eocene. I_s increased markedly at the base of the Castissent interval at 50 Ma, by a factor of 3. This significant increase in sediment intermittency factor suggests sediment transport occurred more frequently and more efficiently in the Castissent Formation. The variation in water intermittency factors across the Montllobat and Castissent intervals was more modest, with a 15-60% reduction of I_w into the Castissent

interval. Considering a theoretical long-term hydrograph (Fig. 15), these results show the integrated area of the sediment hydrograph was greater in the Castissent interval than the previous Montllobat interval for a similar water intermittency.

Intermittency factors make no assumptions on hydrograph shape, only reflecting the integrated area of water or sediment transport beneath the hydrograph curve. However, this shift in I_s permits detailed interpretations of changing hydrological regimes. The observed signal of changing intermittency could be achieved with an enhanced hydrological seasonality that would distribute the same integrated water discharge (similar I_w) such that a greater proportion of the annual water budget in the Castissent rivers was above the threshold for sediment transport (greater I_s) (Fig. 14). The same overall water budget could be maintained whilst the extremes were enhanced, meaning sediment transport could occur in greater volumes, resulting in higher I_s. The changing maximum water and sediment discharge rates that are implied by this inferred change in hydrograph shape, as illustrated in Figure 14, would also be consistent with the palaeohydrological reconstructions of McLeod *et al.* (2025) which showed that $Q_{w(bf)}$ and $Q_{s(bf)}$ increased at the base of the Castissent Formation.

This interpreted change in hydrograph shape is supported by geochemical data acquired from Castissent floodplain deposits which show humidity patterns were strongly seasonal (Honegger *et al.*, 2020). Palaeobotanial proxies also suggest that throughout the early-mid Eocene, Earth's climate was controlled by a global monsoon cycle, driving seasonal precipitation patterns (Greenwood & Huber, 2011). The most likely cause for the observed shift in seasonality and I_s, therefore, is a change in climate. It is well-documented that hyperthermal events caused intense warming for short periods of time in the lower Eocene. There were 39 of these hyperthermals in the early Eocene (Lourens *et al.*, 2005; Kirtland Turner *et al.*, 2014; Westerhold *et al.*, 2018), and it has been hypothesised that at least one of these impacted sedimentation in the Tremp-Graus Basin, causing the observed geochemical and hydrological changes in the Castissent Formation on a timescale of 150-800 kyrs (Honegger *et al.*, 2020; McLeod *et al.*, 2025). These hyperthermal events had widespread effects beyond fluvial

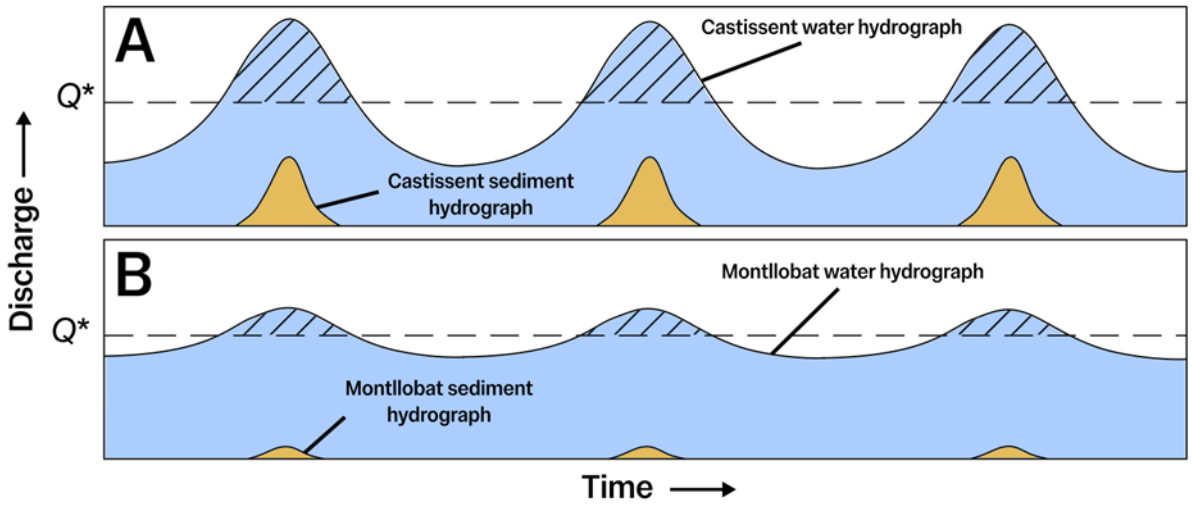

Figure 15. Schematic diagram illustrating theoretical water and sediment hydrographs during (A) the Castissent interval and (B) the Montllobat interval. The blue shaded region indicates the water hydrograph, and the stippled regions represent the integrated area of the water hydrograph above the threshold for sediment transport (*Q**, the dashed line). The yellow shaded region indicates the area of the sediment hydrograph. Two different water hydrograph shapes with the same I_w can result in different I_s.

dynamics, including significant disruption to the carbon cycle and increased terrigenous input to marine basins (Honegger *et al.*, 2020).

Global warming is well-documented to cause reductions in mean annual precipitation and enhanced precipitation extremes in the present-day, especially in arid and semi-arid regions (Goubanova & Li, 2007; Miranda *et al.*, 2011; Quintana-Seguí *et al.*, 2011; Westra *et al.*, 2014; Tramblay & Somot, 2018; He *et al.*, 2022), in addition to enhancing monsoon cycles (Loo *et al.*, 2015). This is observed and projected to cause dramatic increases in sediment loads in semi-arid regions on decadal timescales (McLeod *et al.*, 2024). Whilst mean annual temperatures were gradually decreasing during the Montanyana Group towards the end of the EECO, hyperthermal events could have increased temperatures by 1-3°C on 10^3 yr timescales (Stap *et al.*, 2010; Honegger *et al.*, 2020) resulting in long-term (<10^6 yr) changes to the hydrological cycle, resolvable in the alluvial stratigraphic record.

We hypothesize that increasing I_s into the Castissent interval may be indicative of a significant increase in monsoon seasonality, driven by climate change. Our I_s reconstructions imply sediment could have been in motion as river bedload for at least one week per year: we hypothesise sediment flux was sustained over longer periods in the Castissent interval during

prolonged monsoon discharge above sediment transport thresholds, increasing I_s values. Whilst fossil woody debris are observed in the erosional bases of channel scours (Marzo *et al.*, 1988), there is not abundant evidence of strongly seasonal discharge regimes and seasonally dry river channels such as *in-situ* roots and plant fossils within river channels (Fielding *et al.*, 2009; Plink-Bjorklund, 2015). However, the relatively high I_w of the Montllobat and Castissent formations indicates that channels were most likely not seasonally dry: instead sediment transport thresholds were surpassed only infrequently, meaning sand-transporting conditions may have occurred on a seasonal basis.

Another factor potentially contributing to the observed increase in I_s is a tectonically-driven increase in sediment supply, related to the orogenic evolution of the Pyrenees. In a climate which potentially grew more arid over time, as evidenced by the 15-60% reduction in I_w values (Fig. 11C, D), a change in seasonality could only result in higher I_s on 100 kyr timescales if the system was not supply-limited. McLeod *et al.* (2025) reconstructed greater palaeochannel gradients and bedload grain-sizes in the Castissent Formation, consistent with strong progradation of fluvial facies at c. 50 Ma. An increase in hinterland uplift rates (Curry *et al.*, 2021) likely stimulated increased sediment generation and availability, facilitating more frequent sediment transport in the Castissent rivers.

Our member-level intermittency analyses permit further interpretation of ancient climate change at c. 0.5 Myr resolution (Fig. 11). In each palaeo-routing scenario we observed sediment intermittency starting to increase in the upper Montllobat Formation, peaking in the Castissent A Member at c. 50.5-50.2 Ma before decreasing in the Castissent B and C members. This pattern suggests a discrete change in sediment transport patterns with a duration of 0.8-1.0 Ma before fluvial facies, petrology and inferred hydrological conditions returned to the pre-Castissent baseline (Nijman, 1998). Thus, hyperthermal events, with comparable timescales and magnitudes to current global warming, were the likely cause of a significant change to monsoon seasonality which drove marked fluvial progradation, a marked

increase in sediment transport efficiency, and a reduction of sediment export timescales which lasted up to 1 million years.

It is projected that by 2100 CE river systems in semi-arid regions could experience a doubling of their sediment load as a result of increasing weather extremes (McLeod *et al.*, 2024). Present-day global warming is coupled with major land-use change, a combination that is already dramatically altering the global water and carbon cycle, presenting significant flood and drought hazards to over 3 billion people living on large river corridors (Best, 2019). The lower Eocene represents an example of the long-term consequences of short-term climatic change comparable to current global warming. The ancient river systems of the Montllobat and Castissent formations saw marked changes in water and sediment discharge, morphology and planform, and sediment intermittency, which resulted in heightened sediment transport efficiency and a 20 km downsystem progradation of alluvial facies. Climate change, as evidenced by this ancient example, can cause major geomorphic upheaval from source to sink. Further fluvial geomorphic change in the modern day, on the scales quantified for here for the first time in the Montanyana Group and observed throughout geological history, would have long-lasting consequences for landscapes and communities.

CONCLUSIONS

We reconstructed sediment and water transport patterns in Eocene river systems in an active tectonic setting, the South Pyrenean foreland, which comprised the Tremp-Graus, Ager, Ainsa and Jaca basins, during the Early Eocene Climatic Optimum (EECO), an ancient greenhouse climate punctuated by hyperthermal warming events. In order to estimate river intermittency factors, we calculated long-term sediment fluxes by measuring the total sand-grade depositional volumes of two units in the Montanyana Group of the Tremp-Graus Basin, the Montllobat and Castissent formations, and their down-system equivalents in the Ainsa and Jaca basins. We also reconstructed palaeohydraulics in the rivers of the Corçà Formation to determine channel-forming water and sediment discharge rates through the Àger Basin in addition to the Tremp-Graus Basin. Palaeohydrology of river channel deposits and basin-scale

volumetric reconstructions reveal the rivers of the Montanyana Group had water intermittency factors (I_w) of 0.15-0.25, whereas sediment intermittency factors (I_s) averaging $3x10^{-3}$ – $7x10^{-3}$ in the Montllobat Formation increased 3-fold in the overlying, strongly progradational, Castissent Formation. This suggests that whilst rivers were likely perennial, sand-grade sediment was transported significantly more often in the Castissent rivers, and our data enable us to constrain temporal incompleteness in the geological record. By comparing intermittency results to a global database of modern rivers, we also demonstrate that rivers during the EECO were able to transport sediment more efficiently than most modern rivers of similar types and climate zones today. We hypothesise that short-duration Eocene hyperthermal warming enhanced monsoon seasonality in the Pyrenean foreland, causing significant changes in river behaviour, morphology and style lasting up to 1 million years. Coeval tectonic uplift of the Pyrenean hinterland is also required to increase the supply of available sand. This ancient example shows the long-lasting geomorphic consequences of climatic change with a similar magnitude to present day global warming, impacting timescales of sediment export and landscape dynamics at the mountain-belt scale.

REFERENCES

Alfieri, L., **Bisselink, B.**, **Dottori, F.**, **Naumann, G.**, **de Roo, A.**, **Salamon, P.**, **Wyser, K.** and **Feyen, L.** (2017) Global projections of river flood risk in a warmer world. *Earth's Future*, **5**, 171–182.

Allen, P.A. (2008) From landscapes into geological history. *Nature*, **451**, 274–276.

Ayckbourne, A.J.M., **Jerrett, R.M.**, **Watkinson, M.P.**, **Poyatos-Moré, M.**, **Kane, I.A.**, **Covey-Crump, S.** and **Taylor, K.G.** (2024) Initiation and evolution of an epicontinental shelf-slope margin in an actively contracting deep-water basin: The Eocene Aínsa Basin, southern Pyrenees (Spain). *Basin Research*, **36**, e12884.

Bentham, P. and **Burbank, D.W.** (1996) Chronology of Eocene foreland basin evolution along the western oblique margin of the South–Central Pyrenees. In: *Tertiary Basins of Spain: The Stratigraphic Record of Crustal Kinematics* (Ed. C.J. Dabrio and P.F. Friend), *Cambridge University Press*, Cambridge, 144–152.

Best, J. (2019) Anthropogenic stresses on the world's big rivers. *Nature Geosci*, **12**, 7–21.

Boyrie, C., **Girard, F.**, **Yans, J.**, **Ballas, G.**, **Lihoreau, F.**, **Benammi, M.**, **Bourget, H.**, **Garcia, G.**, **Leredde, C.**, **Pellissier-tanon, A.**, **Valentin, X.**, **Vidalenc, D.** and **Tabuce, R.** (2025) Abrupt changes in continental sedimentation triggered by monsoon-type event during EECO hyperthermals, Minervois Basin, Southern France. *Sedimentary Geology*, 106923.

Bradley, R.W. and **Venditti, J.G.** (2017) Reevaluating dune scaling relations. *Earth-Science Reviews*, **165**, 356–376.

Bull, W.B. (1991) Geomorphic responses to climatic change. *New York, NY (United States); Oxford University Press*.

Cabello, P., **Domínguez, D.**, **Murillo-López, M.H.**, **López-Blanco, M.**, **García-Sellés, D.**, **Cuevas, J.L.**, **Marzo, M.** and **Arbués, P.** (2018) From conventional outcrop datasets and digital outcrop models to flow simulation in the Pont de Montanyana point-bar deposits (Ypresian, Southern Pyrenees). *Marine and Petroleum Geology*, **94**, 19–42.

Caja, M.A., **Marfil, R.**, **Garcia, D.**, **Remacha, E.**, **Morad, S.**, **Mansurbeg, H.**, **Amorosi, A.**, **Martínez-Calvo, C.** and **Lahoz-Beltrá, R.** (2010) Provenance of siliciclastic and hybrid turbiditic arenites of the Eocene Hecho Group, Spanish Pyrenees: implications for the tectonic evolution of a foreland basin. *Basin Research*, **22**, 157–180.

Capote, R., **Muñoz, J.**, **Simón, J.L.**, **Liesa, C.** and **Arlegui, L.** (2002) Alpine tectonics I: The Alpine system north of the Betic Cordillera. *The Geology of Spain*, 367–400.

Chanvry, E., **Deschamps, R.**, **Joseph, P.**, **Puigdefàbregas, C.**, **Poyatos-Moré, M.**, **Serra-Kiel, J.**, **Garcia, D.** and **Teinturier, S.** (2018) The influence of intrabasinal tectonics in the stratigraphic evolution of piggyback basin fills: Towards a model from the Tremp-Graus-Ainsa Basin (South-Pyrenean Zone, Spain). *Sedimentary Geology*, **377**, 34–62.

Clark, J., **Puigdefabregas, C.**, **Castelltort, S.** and **Fildani, A.** (2017) Propagation of Environmental Signals within Source-to-Sink Stratigraphy. *SEPM Society for Sedimentary Geology*.

Cornard, P. and **Pickering, K.** (2020) Submarine topographic control on distribution of supercritical-flow deposits in lobe and related environments, middle Eocene, Jaca Basin, Spanish Pyrenees. *Journal Of Sedimentary Research*, 1222–1243.

Curry, M.E., **Beek, P.V.D.**, **Huismans, R.S.**, **Wolf, S.G.**, **Fillon, C.** and **Muñoz, J.-A.** (2021) Spatio-temporal patterns of Pyrenean exhumation revealed by inverse thermo-kinematic modeling of a large thermochronologic data set. *Geology*, **49**, 738–742.

Dunne, J.P., **Sarmiento, J.L.** and **Gnanadesikan, A.** (2007) A synthesis of global particle export from the surface ocean and cycling through the ocean interior and on the seafloor. Global Biogeochemical Cycles. **6** (3), 583-594.

Engelund, F. and **Hansen, E.** (1967) A monograph on sediment transport in alluvial streams. Technical University of Denmark 0stervoldgade 10, Copenhagen K.

Fielding, C.R., **Alexander, J.** and **Allen, J.P.** (2018) The role of discharge variability in the formation and preservation of alluvial sediment bodies. *Sedimentary Geology*, **365**, 1–20.

Fielding, C.R., **Allen, J.P.**, **Alexander, J.** and **Gibling, M.R.** (2009) Facies model for fluvial systems in the seasonal tropics and subtropics. *Geology*, **37**, 623–626.

Fisher, Q.J., **Casey, M.**, **Clennell, M.B.** and **Knipe, R.J.** (1999) Mechanical compaction of deeply buried sandstones of the North Sea. *Marine and Petroleum Geology*, **16**, 605–618.

Flood, Y.S. and **Hampson, G.J.** (2014) Facies And Architectural Analysis To Interpret Avulsion Style and Variability: Upper Cretaceous Blackhawk Formation, Wasatch Plateau, Central Utah, U.S.A. *Journal of Sedimentary Research*, **84**, 743–762.

Ganti, V., **Whittaker, A.C.**, **Lamb, M.P.** and **Fischer, W.W.** (2019) Low-gradient, single-threaded rivers prior to greening of the continents. *Proceedings of the National Academy of Sciences*, **116**, 11652–11657.

Garcés, M., **López-Blanco, M.**, **Valero, L.**, **Beamud, E.**, **Muñoz, J.A.**, **Oliva-Urcia, B.**, **Vinyoles, A.**, **Arbués, P.**, **Cabello, P.** and **Cabrera, L.** (2020) Paleogeographic and sedimentary evolution of the South Pyrenean foreland basin. *Marine and Petroleum Geology*, **113**, 104105.

Goñi, M.A., **Hatten, J.A.**, **Wheatcroft, R.A.** and **Borgeld, J.C.** (2013) Particulate organic matter export by two contrasting small mountainous rivers from the Pacific Northwest, U.S.A. *Journal of Geophysical Research: Biogeosciences*, **118**, 112–134.

Goubanova, K. and **Li, L.** (2007) Extremes in temperature and precipitation around the Mediterranean basin in an ensemble of future climate scenario simulations. *Global and Planetary Change,* **57**, 27–42.

Greenwood, D.R. and **Huber, M.** (2011) Eocene precipitation: a global monsoon? *American Geophysical Union*, Fall Meeting 2011, San Francisco.

Gupta, K.D. and **Pickering, K.T.** (2008) Petrography and temporal changes in petrofacies of deep-marine Ainsa–Jaca basin sandstone systems, Early and Middle Eocene, Spanish Pyrenees. *Sedimentology*, **55**, 1083–1114.

Haines, A.T., **Finlayson, B.L.** and **McMahon, T.A.** (1988) A global classification of river regimes. *Applied Geography*, **8**, 255–272.

Hansford, M.R., **Plink-Björklund, P.** and **Jones, E.R.** (2020) Global quantitative analyses of river discharge variability and hydrograph shape with respect to climate types. *Earth-Science Reviews*, **200**, 102977.

Hayden, A.T., **Lamb, M.P.** and **McElroy, B.J.** (2021) Constraining the Timespan of Fluvial Activity From the Intermittency of Sediment Transport on Earth and Mars. Geophysical Research Letters. **48**, 16.

He, Y., **Wang, Q.**, **Xu, Y.**, **Li, Z.**, **Yuan, J.**, **Lu, M.** and **Lin, Z.** (2022) Climate change increased the compound extreme precipitation-flood events in a representative watershed of the Yangtze River Delta, China. *Stoch Environ Res Risk Assess*, **36**, 3803–3818.

Hedman, E.R. and **Osterkamp, W.R.** (1982) Streamflow characteristics related to channel geometry of streams in western United States. *U.S. G.P.O.,*.

Honegger, L., **Adatte, T.**, **Spangenberg, J.E.**, **Rugenstein, J.K.C.**, **Poyatos-Moré, M.**, **Puigdefàbregas, C.**, **Chanvry, E.**, **Clark, J.**, **Fildani, A.**, **Verrechia, E.**, **Kouzmanov, K.**, **Harlaux, M.** and **Castelltort, S.** (2020) Alluvial record of an early Eocene hyperthermal within the Castissent Formation, the Pyrenees, Spain. *Clim. Past*, **16**, 227–243.

Hyland, E.G. and **Sheldon, N.D.** (2013) Coupled CO2-climate response during the Early Eocene Climatic Optimum. *Palaeogeography, Palaeoclimatology, Palaeoecology*, **369**, 125–135.

IGME (2013) MAGNA, 1:5000 Series, 2nd Edition. *Instituto Geológico y Minero de España*.

Juvany, P., **Garcés, M.**, **López-Blanco, M.**, **Valero, L.**, **Amorós, E.B.**, **Poyatos-Moré, M.** and **Rius, A.M.** (2024) Unraveling the sediment routing systems evolution of the south Pyrenean foreland basin during the lower to middle Paleogene period. *Marine and Petroleum Geology*, **167**, 106913.

Kim, Y. and **Lee, E.Y.** (2018) Numerical analysis of sedimentary compaction: Implications for porosity and layer thickness variation. **54**, 631–640.

Kirtland Turner, S., **Sexton, P.F.**, **Charles, C.D.** and **Norris, R.D.** (2014) Persistence of carbon release events through the peak of early Eocene global warmth. *Nature Geosci*, **7**, 748–751.

Knox, J.C. (1984) Responses of River Systems to Holocene Climates. In: *Late Quaternary Environments of the United States*, NED-New edition (Ed. H.E. Wright), *University of Minnesota Press*, 26–41.

Knox, J.C. (1993) Large increases in flood magnitude in response to modest changes in climate. *Nature*, **361**, 430–432.

Labaume, P., **Mutti, E.** and **Seguret, M.** (1987) Megaturbidites: A depositional model from the eocene of the SW-Pyrenean Foreland basin, Spain. *Geo-Marine Letters*, **7**, 91–101.

Labaume, P., Meresse, F., Jolivet, M., Teixell, A., Lahfid, A. (2016) Tectonothermal history of an exhumed thrust-sheet-top basin: An example from the south Pyrenean thrust belt. *Tectonics*, 35, 5.

Leclair, S. and **Bridge, J.** (2001) Quantitative Interpretation of Sedimentary Structures Formed by River Dunes. *Journal of Sedimentary Research - J SEDIMENT RES*, **71**, 713–716.

Long, D.G.F. (2021) Trickling down the paleoslope: an empirical approach to paleohydrology. *Earth-Science Reviews*, **220**, 103740.

Loo, Y.Y., **Billa, L.** and **Singh, A.** (2015) Effect of climate change on seasonal monsoon in Asia and its impact on the variability of monsoon rainfall in Southeast Asia. *Geoscience Frontiers*, **6**, 817–823.

Lourens, L.J., **Sluijs, A.**, **Kroon, D.**, **Zachos, J.C.**, **Thomas, E.**, **Röhl, U.**, **Bowles, J.** and **Raffi, I.** (2005) Astronomical pacing of late Palaeocene to early Eocene global warming events. *Nature*, **435**, 1083–1087.

Lyster, S.J., **Whittaker, A.C.**, **Allison, P.A.**, **Lunt, D.J.** and **Farnsworth, A.** (2020) Predicting sediment discharges and erosion rates in deep time—examples from the late Cretaceous North American continent. *Basin Research*, **32**, 1547–1573.

Lyster, S.J., **Whittaker, A.C.**, **Farnsworth, A.** and **Hampson, G.J.** (2023) Constraining flow and sediment transport intermittency in the geological past. *GSA Bulletin*, **136**, 2425–2442.

Lyster, S.J., **Whittaker, A.C.**, **Hampson, G.J.**, **Hajek, E.A.**, **Allison, P.A.** and **Lathrop, B.A.** (2021) Reconstructing the morphologies and hydrodynamics of ancient rivers from source to sink: Cretaceous Western Interior Basin, Utah, USA. *Sedimentology*, **68**, 2854–2886.

Manning, R., **Griffith, J.P.**, **Pigot, T.F.** and **Vernon-Harcourt, L.F.** (1890) On the flow of water in open channels and pipes. 161 pp.

Martín-Chivelet, J., **Berástegui, X.**, **Rosales, I.**, **Vilas, L.**, **Vera, J.A.**, **Caus, E.**, **Gräfe, K.-U.**, **Mas, R.**, **Puig, C.**, **Segura, M.**, **Robles, S.**, **Floquet, M.**, **Quesada, S.**, **Ruiz-Ortiz, P.A.**, **Fregenal-Martínez, M.A.**, **Salas, R.**, **Arias, C.**, **García, A.**, **Martín-Algarra, A.**, **Meléndez, M.N.**, **chacón, B.**, **Molina, J.M.**, **Sanz, J.L.**, **Castro, J.M.**,

García-Hernández, M., **Carenas, B.**, **García-Hidalgo, J.**, **Gil, J.** and **Ortega, F.** (2002) Cretaceous. In: *The Geology of Spain* (Ed. W. Gibbons and T. Moreno), *Geological Society of London*.

Martinius, A. (2012a) Contrasting Styles of Siliciclastic Tidal Deposits in a Developing Thrust-Sheet-Top Basins – The Lower Eocene of the Central Pyrenees (Spain). In: *Principles of Tidal Sedimentology*, 473–506.

Martinius, A.W. (2012b) Contrasting Styles of Siliciclastic Tidal Deposits in a Developing Thrust-Sheet-Top Basins – The Lower Eocene of the Central Pyrenees (Spain). In: *Principles of Tidal Sedimentology* (Ed. R.A. Davis and R.W. Dalrymple), *Springer Netherlands*, Dordrecht, 473–506.

Marzo, M., **Nijman, W.** and **Puigdefabregas, C.** (1988) Architecture of the Castissent fluvial sheet sandstones, Eocene, South Pyrenees, Spain. *Sedimentology*, **35**, 719–738.

McLeod, J.S., **Ganti, V.**, **Hampson, G.J.**, **Bell, R.E.**, **Slater, L.J.**, **Liu, Y.**, **Rees, H.C.** and **Whittaker, A.C.** (2026) Global sediment transport intermittency is set by river planform. *Nat. Geosci.,* (in review).

McLeod, J.S., **Whittaker, A.C.**, **Bell, R.E.**, **Hampson, G.J.**, **Watkins, S.E.**, **Brooke, S.A.S.**, **Rezwan, N.**, **Hook, J.**, **Zondervan, J.R.**, **Ganti, V.** and **Lyster, S.J.** (2024) Landscapes on the edge: River intermittency in a warming world. *Geology*, **52**, 512–516.

McLeod, J.S., **Whittaker, A.C.**, **Hampson, G.J.**, **Bell, R.E.**, **Prieur, M.**, **Fuller-Field, O.G.**, **Valero, L.**, **Yan, X.** and **Valenza, J.M.** (2025) Hothouse Hydrology: Evolving River Dynamics in the Eocene Montllobat and Castissent Formations, Southern Pyrenees. *Basin Research*, **37**, e70059.

McLeod, J.S., **Wood, J.**, **Lyster, S.J.**, **Valenza, J.M.**, **Spencer, A.R.T.** and **Whittaker, A.C.** (2023) Quantitative constraints on flood variability in the rock record. *Nat Commun*, **14**, 3362.

Meyer-Peter, E. and **Müller, R.** (1948) Formulas for Bed-Load transport. In: *IAHSR 2nd meeting, Stockholm, appendix 2*.

Miall, A.D. (2015) Updating uniformitarianism: stratigraphy as just a set of 'frozen accidents.' *Geological Society of London, Special Publications*, **404**, 11–36.

Miranda, J.D., **Armas, C.**, **Padilla, F.M.** and **Pugnaire, F.I.** (2011) Climatic change and rainfall patterns: Effects on semi-arid plant communities of the Iberian Southeast. *Journal of Arid Environments*, **75**, 1302–1309.

Mochales, T., **Barnolas, A.**, **Pueyo, E.L.**, **Serra-Kiel, J.**, **Casas, A.M.**, **Samsó, J.M.**, **Ramajo, J.** and **Sanjuán, J.** (2012) Chronostratigraphy of the Boltaña anticline and the Ainsa Basin (southern Pyrenees). *GSA Bulletin*, **124**, 1229–1250.

Muñoz, J.A., **Izquierdo-Llavall, E.**, **Santolaria, P.**, **Toro, R.**, **Pueyo, E.L.**, **Casas, A.M.** and **Granado, P.** (2025) Inheritance in shortening transfer and kinematics in fold-and-thrust belts: Revisiting the structure of the Jaca Basin, Southern Pyrenees. *Earth-Science Reviews*, **270**, 105237.

Muto, T., **Steel, R.J.** and **Swenson, J.B.** (2007) Autostratigraphy: A Framework Norm for Genetic Stratigraphy. *Journal of Sedimentary Research*, **77**, 2–12.

Mutti, E. (1985a) Hecho Turbidite System, Spain. In: *Submarine Fans and Related Turbidite Systems*, 205–208.

Mutti, E. (1985b) Turbidite Systems and Their Relations to Depositional Sequences. *Provenance of arenites. Proc. Cetraro, Cosenza, 1984*, 65–93.

Mutti, E. (1985c) Stratigraphy and facies characteristics of the Eocene Hecho Group turbidite systems, south-central Pyrenees. *IAS*, Lleida [i.e. Lérida, Spain].

Nicholas, A.P., **Sambrook Smith, G.H.**, **Amsler, M.L.**, **Ashworth, P.J.**, **Best, J.L.**, **Hardy, R.J.**, **Lane, S.N.**, **Orfeo, O.**, **Parsons, D.R.**, **Reesink, A.J.H.**, **Sandbach, S.D.**, **Simpson, C.J.** and **Szupiany, R.N.** (2016) The role of discharge variability in determining alluvial stratigraphy. *Geology*, **44**, 3–6.

Nijman, W. (1990) Thrust sheet rotation ? — The South Pyrenean Tertiary basin configuration reconsidered. *Geodinamica Acta*, **4**, 17–42.

Nijman, W. (1998) Cyclicity and basin axis shift in a piggyback basin: towards modelling of the Eocene Tremp-Ager Basin, South Pyrenees, Spain. *Geological Society of London Special Publication*, **134**, 135–162.

Nijman, W. and **Nio, S.D.** (1975) The Eocene Montañana Delta: Tremp-Graus Basin, Provinces of Lérida and Huesca, Southern Pyrenees, N. Spain). *Vakgroep Sedimentologie, Rijksuniveriteit Leiden-Utrecht*, 20 pp.

Nijman, W. and **Puigdefàbregas, C.** (1977) Coarse-Grained Point Bar Structure in a Molasse-Type Fluvial System, Eocene Castisent Sandstone Formation, South Pyrenean Basin.

Oliva-Urcia, B., Beamud, E., Arenas, C., Pueyo, E.L., Garcés, M., Soto, R., Valero, L. and Pérez-Rivarés, F.J. (2019). Dating the northern deposits of the Ebro foreland basin; implications for the kinematics of the SW Pyrenean front. *Tectonophysics*, 765, pp.11-34.

Ott, R.F., **Kober, F.**, **Ivy-Ochs, S.**, **Scherler, D.**, **von Blanckenburg, F.**, **Christl, M.** and **Vockenhuber, C.** (2025) Erosion-weathering partitioning from paired-mineral and weathering-corrected cosmogenic nuclide approaches. *Quaternary Science Reviews*, **348**, 109114.

Paola, C. (2016) A Mind of Their Own: Recent Advances in Autogenic Dynamics in Rivers and Deltas. SEPM Special Publication. doi: 10.2110/sepmsp.106.04

Paola, C., **Ganti, V.**, **Mohrig, D.**, **Runkel, A.C.** and **Straub, K.M.** (2018) Time Not Our Time: Physical Controls on the Preservation and Measurement of Geologic Time. *Annual Review of Earth and Planetary Sciences*, **46**, 409–438.

Paola, C., **Heller, P.L.** and **Angevine, C.L.** (1992) The large-scale dynamics of grain-size variation in alluvial basins, 1: Theory. *Basin Research*, **4**, 73–90.

Payros, A., **Tosquella, J.**, **Bernaola, G.**, **Dinarès-Turell, J.**, **Orue-Etxebarria, X.** and **Pujalte, V.** (2009) Filling the North European Early/Middle Eocene (Ypresian/Lutetian) boundary gap: Insights from the Pyrenean continental to deep-marine record. *Palaeogeography, Palaeoclimatology, Palaeoecology*, **280**, 313–332.

Phillips, C.B. and **Jerolmack, D.J.** (2019) Bankfull Transport Capacity and the Threshold of Motion in Coarse-Grained Rivers. *Water Resour. Res.*, **55**, 11316–11330.

Plink-Bjorklund, P. (2015) Morphodynamics of rivers strongly affected by monsoon precipitation: Review of depositional style and forcing factors. Sedimentary Geology. **323**.

Poyatos-More, M. (2014) Physical Stratigraphy and Facies Analysis of the Castissent Tecto-Sedimentary Unit (South-Central Pyrenees, Spain): Depositional processes and controlling factors of sediment dispersal from river-mouth to base-of-slope settings. Unpublished PhD Thesis.

Puigdefabregas, C. and **Vliet, A.V.** (1977) Meandering Stream Deposits From the Tertiary of the Southern Pyrenees. In: *Fluvial Sedimentology - Memoir 5*, *Dallas Geological Society*, 469–485.

Quintana-Seguí, P., **Habets, F.** and **Martin, E.** (2011) Comparison of past and future Mediterranean high and low extremes of precipitation and river flow projected using different statistical downscaling methods. *Nat. Hazards Earth Syst. Sci.*, **11**, 1411–1432.

Raimat Quintana, C., **Remacha Grau, E.**, **Oms Llobet, O.** and **Cardona Arboleda, O.D.** (1997) Presencia del Alogrupo de Figols en las turbiditas de la base del Grupo de Hecho (Barranco del Sorrosal, Prov. de Huesca). *Geogaceta*, 179–182.

Remacha, E. and **Fernández, L.P.** (2003) High-resolution correlation patterns in the turbidite systems of the Hecho Group (South-Central Pyrenees, Spain). *Marine and Petroleum Geology*, **20**, 711–726.

Remacha, E., **Fernández, L.P.** and **Maestro, E.** (2005) The Transition Between Sheet-Like Lobe and Basin-Plain Turbidites in the Hecho Basin (South-Central Pyrenees, Spain). *Journal of Sedimentary Research*, **75**, 798–819.

Roigé, M., **Gómez-Gras, D.**, **Teixell, A.**, **Coll, X.** and **Boya, S.** (2026) The Source-to-Sink Evolution of the Jaca Basin (Southern Pyrenees). In: *Evolution of the Pyrenees during the Variscan and Alpine Cycles 2*, 131–159.

Sadler, P.M. (1981) Sediment Accumulation Rates and the Completeness of Stratigraphic Sections. *The Journal of Geology*, **89**, 569–584.

Sambrook Smith, G.H., **Best, J.L.**, **Ashworth, P.J.**, **Lane, S.N.**, **Parker, N.O.**, **Lunt, I.A.**, **Thomas, R.E.** and **Simpson, C.J.** (2010) Can we distinguish flood frequency and magnitude in the sedimentological record of rivers? *Geology*, **38**, 579–582.

Schlumberger (2017) Petrel Manual. *Petrel Schlumberger*.

Schoonejans, J., **Vanacker, V.**, **Opfergelt, S.**, **Ameijeiras-Mariño, Y.** and **Christl, M.** (2016) Kinetically limited weathering at low denudation rates in semiarid climatic conditions. *Journal of Geophysical Research: Earth Surface*, **121**, 336–350.

Scotchman, J.I., **Bown, P.**, **Pickering, K.T.**, **BouDagher-Fadel, M.**, **Bayliss, N.J.** and **Robinson, S.A.** (2015) A new age model for the middle Eocene deep-marine Ainsa Basin, Spanish Pyrenees. *Earth-Science Reviews*, **144**, 10–22.

Seguret, M., **Labaume, P.** and **Madariaga, R.** (1984) Eocene seismicity in the Pyrenees from megaturbidites of the South Pyrenean Basin (Spain). *Marine Geology*, **55**, 117–131.

Stap, L., **Lourens, L.J.**, **Thomas, E.**, **Sluijs, A.**, **Bohaty, S.** and **Zachos, J.C.** (2010) High-resolution deep-sea carbon and oxygen isotope records of Eocene Thermal Maximum 2 and H2. *Geology*, **38**, 607–610.

Syvitski, J.P.M. and **Milliman, J.D.** (2007) Geology, Geography, and Humans Battle for Dominance over the Delivery of Fluvial Sediment to the Coastal Ocean | The Journal of Geology: Vol 115, No 1. **115**, 1–19.

Thomson, K.D., **Stockli, D.F.**, **Clark, J.D.**, **Puigdefàbregas, C.** and **Fildani, A.** (2017) Detrital zircon (U-Th)/(He-Pb) double-dating constraints on provenance and foreland basin evolution of the Ainsa Basin, south-central Pyrenees, Spain. *Tectonics*, **36**, 1352–1375.

Tramblay, Y. and **Somot, S.** (2018) Future evolution of extreme precipitation in the Mediterranean. *Climatic Change*, **151**, 289–302.

Trampush, S.M., **Huzurbazar, S.** and **McElroy, B.** (2014) Empirical assessment of theory for bankfull characteristics of alluvial channels. *Water Resources Research*, **50**, 9211–9220.

Tucker, G.E. and **Slingerland, R.** (1997) Drainage basin responses to climate change. *Water Resources Research*, **33**, 2031–2047.

Turner, S.K. (2018) Constraints on the onset duration of the Paleocene-Eocene Thermal Maximum. *Philos Trans A Math Phys Eng Sci*, **376**, 20170082.

Van der Meulen, S. (1989) The distribution of Pyrenean erosion material, deposited by eocene sheetflood systems and associated fan-deltas : a fossil record in the Monllobat and adjacent Castigaleu formations, in the drainage area of the present Rio Noguerra Ribagorzana, provinces of Huesca and Lérida, Spain. *Rijksuniversiteit, Mineralogisch-geologisch instituut*.

Van Der Meulen, S. (1986) Eocene sheetflood systems and transitional fan-deltas, Southern Pyrenees, Spain. *Geological Journal*, **21**, 169–199.

Van Eden, J.G. (1970) A reconnaissance of deltaic environment in the middle Eocene of the south-central Pyrenees, Spain. **49**, 145–157.

Vinyoles, A., **López-Blanco, M.**, **Garcés, M.**, **Arbués, P.**, **Valero, L.**, **Beamud, E.**, **Oliva-Urcia, B.** and **Cabello, P.** (2021) 10 Myr evolution of sedimentation rates in a deep marine to non-marine foreland basin system: Tectonic and sedimentary controls (Eocene, Tremp–Jaca Basin, Southern Pyrenees, NE Spain). *Basin Research*, **33**, 447–477.

Wang, D. and **Alimohammadi, N.** (2012) Responses of annual runoff, evaporation, and storage change to climate variability at the watershed scale. *Water Resources Research*. **48**, W05546

Watkins, S.E., **Whittaker, A.C.**, **Bell, R.E.**, **Brooke, S.A.S.**, **Ganti, V.**, **Gawthorpe, R.L.**, **McNeill, L.C.** and **Nixon, C.W.** (2020) Straight from the source's mouth: Controls on

field-constrained sediment export across the entire active Corinth Rift, central Greece. *Basin Res*, **32**, 1600–1625.

Watkins, S.E., **Whittaker, A.C.**, **Bell, R.E.**, **McNeill, L.C.**, **Gawthorpe, R.L.**, **Brooke, S.A.S.** and **Nixon, C.W.** (2019) Are landscapes buffered to high-frequency climate change? A comparison of sediment fluxes and depositional volumes in the Corinth Rift, central Greece, over the past 130 k.y. *GSA Bulletin*, **131**, 372–388.

Wentworth, C.K. (1922) A Scale of Grade and Class Terms for Clastic Sediments. *The Journal of Geology*, **30**, 377–392.

Westerhold, T. and **Röhl, U.** (2009) High resolution cyclostratigraphy of the early Eocene – new insights into the origin of the Cenozoic cooling trend. *Climate of the Past*, **5**, 309–327.

Westerhold, T., **Röhl, U.**, **Donner, B.** and **Zachos, J.C.** (2018) Global Extent of Early Eocene Hyperthermal Events: A New Pacific Benthic Foraminiferal Isotope Record From Shatsky Rise (ODP Site 1209). *Paleoceanography and Paleoclimatology*, **33**, 626–642.

Westerhold, T., **Röhl, U.**, **Frederichs, T.**, **Agnini, C.**, **Raffi, I.**, **Zachos, J.C.** and **Wilkens, R.H.** (2017) Astronomical calibration of the Ypresian timescale: implications for seafloor spreading rates and the chaotic behavior of the solar system? *Climate of the Past*, **13**, 1129–1152.

Westra, S., **Fowler, H.J.**, **Evans, J.P.**, **Alexander, L.V.**, **Berg, P.**, **Johnson, F.**, **Kendon, E.J.**, **Lenderink, G.** and **Roberts, N.M.** (2014) Future changes to the intensity and frequency of short-duration extreme rainfall. *Rev. Geophys.*, **52**, 522–555.

Whitchurch, A.L., **Carter, A.**, **Sinclair, H.D.**, **Duller, R.A.**, **Whittaker, A.C.** and **Allen, P.A.** (2011) Sediment routing system evolution within a diachronously uplifting orogen:

Insights from detrital zircon thermochronological analyses from the South-Central Pyrenees. *American Journal of Science*, **311**, 442–482.

Whittaker, A.C. (2012) How do landscapes record tectonics and climate? *Lithosphere*, **4**, 160–164.

Wolman, M.G. (1954) A method of sampling coarse river-bed material. *Eos, Transactions American Geophysical Union*, **35**, 951–956.

Wood, J., **McLeod, J.S.**, **Lyster, S.J.** and **Whittaker, A.C.** (2022) Rivers of the Variscan Foreland: fluvial morphodynamics in the Pennant Formation of South Wales, UK. *Journal of the Geological Society*, **180**, jgs2022-048.

Yan, X., **Whittaker, A.C.** and **Gréselle, B.** (2025) Reconciling Geologic and Paleotopographic Constraints on Source-to-Sink Sediment Fluxes: An Example From the Bartonian Pyrenees. *Basin Research*, **37**, e70037.

Yin, S., **Gao, G.**, **Ran, L.**, **Li, D.**, **Lu, X.** and **Fu, B.** (2023) Extreme streamflow and sediment load changes in the Yellow River Basin: Impacts of climate change and human activities. *Journal of Hydrology*, **619**, 129372.

Figure/Table captions

Figure 1. Diagrams outlining intermittency factors. A) Conceptual illustration highlighting the intermittency factor formula and its inputs where source — or upstream — approaches are used to estimate precipitation and erosion rates, sink — or downstream — approaches are used to estimate deposition rate, and palaeohydrology of alluvial deposits are used to estimate bankfull water and sediment transport capacity. B) Schematic hydrograph illustrating the potential hydrograph shapes for a low intermittency factor of I=0.1, where t_1-t_0 is an arbitrary time-step containing variability, for example 1 year; the blue area represents the water hydrograph and the beige area represents the sediment hydrograph. As long as the integrated area of the hydrograph is maintained, a given intermittency factor could indicate an infinite number of hydrograph shapes. C) Schematic hydrograph illustrating the potential hydrograph shapes for a high intermittency factor of I=0.7. (D-E) Photographs of ephemeral rivers in Greece at bankfull discharge (D) and during low or no flow stages (E) (McLeod *et al.*, 2024)

Figure 2. Study area geological and location maps in the southern Pyrenees. A) Geological sketch map highlighting the key sedimentary units of the Ypresian. B) Digital elevation model of the present-day Pyrenees. C) Geographical location map.

Figure 3. Stratigraphic framework for the lower Eocene units of the southern Pyrenean foreland in the Jaca, Ainsa, Tremp-Graus and Àger basins (modified after Mutti, 1985a; Labaume *et al.*, 1987; Gupta & Pickering, 2008; Caja *et al.*, 2010; Scotchman *et al.*, 2015; Garcés *et al.*, 2020). Variations on this framework could arise from different age-date interpretations and unit correlations. An alternative correlative scheme is provided in the Supplementary Material and discussed in Section 5.2.

Figure 4. Sand thickness dataset locations for the (A) Castissent Formation and correlative strata (Fig. 3), and (B) Montllobat Formation and correlative strata (Fig. 3). Data points are coloured according to total sand deposit thickness. See Supplementary Material (section S2) for the full thickness dataset.

Figure 5. Exposures of the fluvial Montllobat, Castissent and Corçà formations at (A, D, G) channel scale; (B, E, H) bedform-scale; and (C, F, I) grain-scale. Coloured outlines highlight interpreted alluvial architectural features where green represents barform-bounding surfaces, blue represents barform-accretion surfaces and yellow represents dune-scale cross-set bounding surfaces. See Supplementary Material (Fig. S1) for an unannotated version.

Figure 6. Palaeo-sediment routing scenarios for the Montllobat and Castissent intervals, highlighting two alternative scenarios for the source-to-sink palaeogeography of the Montllobat and Corçà rivers (Montllobat Scenarios A and B) and for the Castissent and Corçà rivers (Castissent Scenarios A and B) in the early Eocene south central unit of the Pyrenean foreland.

Figure 7. Sand volume isochores. (A) The structural and palaeogeographic context of the depositional sand volumes in the southern Pyrenean foreland superimposed on the minimum sand volume for Castissent-age strata (Fig. 7C), where the black line represents the palaeogeographic extent of the Tremp-Graus-Ainsa-Jaca basin (modified after Remacha et al. (2005)) and the red lines represent major thrust faults (N = Nogueres, B = Boixols, SPF = South Pyrenean Front). The volume is coloured according to total sand thickness. (B) The maximum and (C) minimum sand volumes for Castissent-age strata, where the white circles represent the thickness dataset. (D) The maximum and (E) minimum sand volume for the Montllobat-age strata. See Supplementary Materials (section S2) for sediment thickness data.

Figure 8. Downsystem sand-grade sediment volumetrics. (A) The sand volume along a downsystem transect (X-X' in Fig. 7A), where the Castissent-age volume is overlaid on the Montllobat volume. Uncertainty margins are based on the volume range within 15 km boxes along the transect, according to methodology for our topography approach (Methods). (B) The cumulative sand volume for each formation.

Figure 9. Corçà Formation palaeohydrology. (A) Bedform-derived palaeo-flow depth, (B) reconstructed palaeo-channel gradient, and (C) total flow width at bankfull.

Figure 10. River discharge in the Tremp-Graus and Àger basins. (A) Total water discharge, and (B) total sediment discharge in the Montllobat (yellow), Castissent (blue) and Corçà (pink) formations.

Figure 11. Evolving intermittency factors through time. (A) Sediment intermittency factors reconstructed using palaeo-routing Scenario A (Fig. 4), where boxplots represent average intermittency factors in the Montllobat and Castissent formations, and the evolution chart illustrates the changing I_s through time between members of the Montllobat and Castissent formations (x-axis). (B) Corresponding sediment intermittency factors reconstructed using palaeo-routing Scenario B (Fig. 4). (C, D) Water intermittency factors reconstructed using (C) palaeo-routing Scenario A and (D) palaeo-routing Scenario B (Fig. 4).

Figure 12. Comparison between sediment intermittency factors estimated for Castissent rivers using our approach outlined, and estimates from a BQART-derived equivalent.

Figure 13. Comparison of intermittency factors for Montllobat and Castissent rivers with those for a global dataset of modern rivers (McLeod *et al.*, 2026).

Figure 14. Cumulative probability functions of intermittency factors for a global compilation of modern rivers (McLeod *et al.*, 2026). (A) The cumulative probability functions of I_w and I_s for modern rivers of all planform types, with intermittency factor values for the Eocene Montllobat and Castissent rivers superimposed. (B) The cumulative probability function for modern braided rivers, with intermittency factors for Castissent rivers shown for comparison. (C) The cumulative probability function for modern wandering rivers, with intermittency factors for Montllobat rivers superimposed.

Figure 15. Schematic diagram illustrating theoretical water and sediment hydrographs during (A) the Castissent interval and (B) the Montllobat interval. The blue shaded region indicates the water hydrograph, and the stippled regions represent the integrated area of the water hydrograph above the threshold for sediment transport (Q^*, the dashed line). The yellow shaded region indicates the area of the sediment hydrograph. Two different water hydrograph shapes with the same I_w can result in different I_s.